# High peatland methane emissions following permafrost thaw: enhanced acetoclastic methanogenesis during early successional stages

Liam Heffernan[1,2*]★, Maria A. Cavaco[3*]★, Maya P. Bhatia[3], Cristian Estop-Aragonés[4], Klaus-Holger Knorr[4], David Olefeldt[1]

[1] Department of Renewable Resources, University of Alberta, Edmonton, AB T6G 2H1, Canada. [2] Evolutionary Biology Centre, Department of Ecology and Genetics/Limnology, Uppsala University, Norbyvägen 18D, 752 36, Uppsala, Sweden. [3] Department of Earth and Atmospheric Sciences, University of Alberta, Edmonton, AB T6G 2H1, Canada. [4] Institute of Landscape Ecology, Ecohydrology and Biogeochemistry Group, University of Münster, Münster, Germany

[*]Corresponding authors**:** Liam Heffernan (liam.heffernan@ebc.uu.se) and Maria A. Cavaco (cavaco@ualberta.ca)

★ These authors contributed equally to this work

## Abstract

Permafrost thaw in northern peatlands often leads to increased methane ($CH_4$) emissions, but the underlying controls responsible for increased emissions and the duration for which they persist have yet to be fully elucidated. We assessed how shifting environmental conditions affect microbial communities, and the magnitude and stable isotopic signature ($\delta^{13}C$) of $CH_4$ emissions along a thermokarst bog transect in boreal western Canada. Thermokarst bogs develop following permafrost thaw when dry, elevated peat plateaus collapse and become saturated and dominated by *Sphagnum* mosses. We differentiated between a young and a mature thermokarst bog stage (~30 and ~200 years since thaw, respectively). The young bog located along the thermokarst edge, was wetter, warmer and dominated by hydrophilic vegetation compared to the mature bog. Using high throughput 16S rRNA gene sequencing, we show that microbial communities were distinct near the surface and converged with depth, but lesser differences remained down to the lowest depth (160 cm). Microbial community analysis and $\delta^{13}C$ data from $CH_4$ surface emissions and dissolved gas depth profiles show that hydrogenotrophic methanogenesis was the dominant pathway at both sites. However, mean $\delta^{13}C$-$CH_4$ signatures of both dissolved gases profiles and surface $CH_4$ emissions were found to be isotopically heavier in the young bog (-63 ‰ and -65 ‰, respectively) compared to the mature bog (-69 ‰ and -75 ‰, respectively), suggesting that acetoclastic methanogenesis was relatively more enhanced throughout the young bog peat profile. Furthermore, mean young bog $CH_4$ emissions of 82 mg $CH_4$ $m^{-2}$ $day^{-1}$, were ~ three times greater than the 32 mg $CH_4$ $m^{-2}$ $day^{-1}$, observed in the mature bog. Our study suggests that interactions between the methanogenic community, hydrophilic vegetation, warmer temperatures, and saturated surface conditions enhance $CH_4$ emissions in young thermokarst bogs, but that these favorable conditions only persist for the initial decades after permafrost thaw.

**Keywords**

Permafrost, peatland, thermokarst, 16S RNA, isotope, methanogenesis, microbial community, methane emissions

## 1. Introduction

Methane ($CH_4$) emissions in northern peatlands are typically thought to be driven by environmental and ecological conditions such as temperature, water table position, and vegetation community (Bellisario et al., 1999). However, $CH_4$ emissions are ultimately the result of microbial activity and understanding the interactions between environmental conditions and microbial processes is key to understanding the impact of disturbances on peatland $CH_4$ emissions. Increased disturbances such as permafrost thaw are transforming northern latitude peatlands (Helbig, Pappas & Sonnentag, 2016), through the disruption of the frozen landscape and environmental conditions responsible for the regional accumulation of large peatland carbon (C) stores. Rapidly rising northern air temperatures (Mudryk et al., 2018) are predicted to lead to widespread gradual thawing of permafrost (Schaefer et al., 2011) and subsequent thermokarst development in high C density permafrost peatlands (Olefeldt et al., 2016). Thermokarst formation in ice-rich permafrost peatlands is characterized by ground subsidence and surface inundation (Camill, 1999). This exposes previously frozen C to anaerobic microbial decomposition and potential mineralization into greenhouse gases (Schuur et al., 2015). Redox conditions following thermokarst formation are an important control of decomposition, with 3 – 4 times greater C mineralization occurring as aerobic respiration compared to anaerobic respiration (Schädel et al., 2016). Increased emissions of methane ($CH_4$) due to thermokarst formation are projected to result in a positive feedback with climate warming (Turetsky et al., 2020). However, the magnitude of peatland $CH_4$ emissions and the metabolic pathways responsible for these emissions in

response to permafrost thaw remain uncertain, as does the period for which these conditions and emissions persist.

Methanogenesis, conducted by methanogenic archaea belonging to phylum Euryarchaeota, is one of the most prominent microbial processes contributing to the anaerobic decomposition of organic matter in water-logged permafrost soils (Cai et al., 2016; Knoblauch et al., 2018). Methanogenesis occurs primarily via two pathways: acetoclastic methanogenesis and hydrogenotrophic methanogenesis (Whiticar et al., 1986; Whiticar, 1999). Acetoclastic methanogenesis involves the cleavage of acetate into $CH_4$ and $CO_2$ and when considering these two species, causes less apparent fractionation than the hydrogenotrophic methanogenesis pathway. This results in acetoclastic methanogenesis yielding comparatively isotopically heavy $\delta^{13}C$-$CH_4$ ($\delta^{13}C$ = -65 to -50‰). The reduction of $CO_2$ and $H_2$ in hydrogenotrophic methanogenesis typically produces $CH_4$ lighter in $^{13}C$ ($\delta^{13}C$ = -110 to -60‰) (Hornibrook et al., 1997, 2000). While the two pathways are stoichiometrically equal (Conrad, 1999; Corbett et al., 2013), the activity of acetoclastic and hydrogenotrophic methanogens are governed by different extrinsic controls (Bridgham et al., 2013).

Hydrogenotrophic methanogenesis is thought to be the main pathway of $CH_4$ formation in northern peatlands (Hornibrook et al., 1997; Galand et al., 2005). However, the acetoclastic pathway can dominate in the upper layers of more minerotrophic, nutrient rich peatlands (Popp et al., 1999; Chasar et al., 2000) where there are sufficient levels of acetate (Ye et al., 2012). During the initial decades following thaw, surface runoff of nutrients from surrounding intact peat plateaus (Keuper et al., 2012; 2017) and increased connectivity to regional hydrology (Connon et al., 2014), can result in more minerotrophic conditions. Such shifts in hydrology, temperature, nutrients, redox conditions, and vegetation communities following permafrost thaw have been shown to increase the prevalence of acetoclastic

methanogenesis and $CH_4$ emissions (Hodgkins et al., 2014; McCalley et al., 2014). However, this potential post-thaw enhancement of acetoclastic methanogenesis needs to be considered in context of the existing methanogenic community that developed in the peat profile before thaw. For example, historical environmental conditions have been shown to have a legacy effect on the methanogenic community following thaw and can therefore be a key constraint on methanogenic community structure and activity post-thaw (Holm et al., 2020; Lee et al., 2012). Overall, an understanding of the methanogenic community's response following thaw to shifts in both surface conditions and exposure to previously frozen organic matter is key to estimating $CH_4$ emissions from thermokarst peatlands.

Environmental conditions following permafrost thaw in peatlands are characterized by a drastic shift in water table position and increased wetness, increased soil temperatures, and a change in vegetation community associated with increased labile inputs (Beilman, 2001; Burd et al., 2020; Camill, 1999). These shifts may provide optimal conditions for $CH_4$ production and emissions, particularly in the initial decades following thaw. Peatland $CH_4$ emissions are constrained by water table position (Huang et al., 2021; Strack et al., 2004), and surface inundation leads to increased $CH_4$ emissions (Tuittila et al., 2000). Methane production and emissions are positively influenced by soil temperatures (Hopple et al., 2020; Olefeldt et al., 2017), and peatland $CH_4$ emissions have been shown to increase when both water table position and temperatures are high (Grant, 2015). The colonization of vegetation associated with fresh, labile inputs has also been shown to increase both the magnitude and temperature sensitivity of $CH_4$ emissions in peatlands (Leroy et al., 2017; McNicol et al., 2019). As such, many studies have focussed on the relationship between water table position, soil temperature and vegetation communities in determining $CH_4$ fluxes following thaw (Johnston et al., 2014; Turetsky et al., 2007; Wickland et al., 2006). However, while these environmental conditions are key drivers of $CH_4$ emissions, they are unable to fully account

for the variability in permafrost peatland $CH_4$ emissions (Juottonen et al., 2021; Kuhn et al., 2021). Some of this unaccounted variance may be in part explained by microbial activity, as changes in the composition and abundance of methanogenic community members can contribute significantly towards peatland $CH_4$ emissions (Fritze et al., 2021). Relatively few studies have assessed how shifts in environmental conditions and ensuing changes in methanogenic community structure influences $CH_4$ emissions following thaw (McCalley et al., 2014), an interaction that may be significant both at the local and circumpolar scale.

In this study we assess the impact of permafrost thaw on peatland methanogenic community composition and $CH_4$ emissions along a space-for-time thaw gradient that includes an intact peat plateau and an adjacent thermokarst bog with areas that have thawed ~30 and ~200 years ago (herein referred to as young bog and mature bog, respectively). Thermokarst formation has resulted in distinct environmental conditions at each stage along this thaw gradient. We herein define these distinct environmental conditions as water table position and surface wetness, soil temperatures, and vegetation community. Along this gradient we assessed methanogenic community structure down to 160 cm. We hypothesize that: (1) shifting environmental conditions along the permafrost thaw gradient results in a successional microbial community and a restructuring of the methanogenic community, and (2) the warmer conditions and hydrophilic vegetation community in the young bog, along with the exposure of previously frozen peat, will result in a greater relative abundance of acetoclastic methanogens throughout the depth profile, and subsequently greater overall $CH_4$ emissions. In the young bog and mature bog, we measured the concentration and $\delta^{13}C$-signature of dissolved $CH_4$ and $CO_2$ down to 245 cm, and the rates and $\delta^{13}C$-signature of both $CH_4$ and $CO_2$ land-atmosphere fluxes. The combined approach of measuring dissolved gas depth profiles and surface emissions, in tandem with assessing the structure of the methanogenic community along a depth profile, allows us to determine how changing

environmental conditions following thaw impacts methanogenic pathways and community composition. Utilizing this approach, we can subsequently gain further insight into how long elevated surface $CH_4$ emissions may persist post-thaw. Furthermore, this approach highlights that while environmental and environmental conditions are important in determining $CH_4$ emissions, microbial community composition, and changes in the methanogenic community structure are likely to significantly influence $CH_4$ emissions following thaw.

## 2. Methods

### *2.1 Study Site and Design*

The Lutose peatland study site (59.5°N, 117.2°W; Figure 1) is located on the Interior Plains of western Canada, within the zone of discontinuous permafrost (Brown et al., 1997; Heginbottom et al., 1995). The climate is continental with a monthly average summer high temperature of 16.1 °C (July), winter low of -22.8 °C (January), and annual average air temperature of -1.8 °C (Climate-Data.org, 2019 – data from site located ~50 km south of Lutose). Annual average precipitation is 391 mm, of which three quarters fall as rain between May and September. In the discontinuous permafrost zone of the Interior Plains in boreal western Canada, ~40% of the landscape is covered by permafrost peatlands that have between 2 and 6 m deep peat deposits (Gibson et al., 2018; Vitt et al., 2000). The peatland complexes in this area are a fine-scale mosaic of permafrost peat plateaus, and permafrost-free ponds, fens, and bogs (Zoltai, 1993; Bauer et al., 2003; Vitt et al., 2000; Pelletier et al., 2017), and they are similar to those found in the Hudson Bay Lowlands (Kuhry, 2008) and Alaska (Jones et al., 2017). The Lutose peatland complex is representative of the peatlands found in the discontinuous permafrost zone of the Interior Plains in western Canada (Heffernan et al., 2020). The site has 5 – 6 m deep peat and has transitioned through multiple developmental stages since it began accumulating organic matter ~8,800 years ago. It

transitioned from a marsh, through a fen and a bog stage prior to permafrost aggradation ~1,800 years ago (Heffernan et al., 2020). Peatlands in the Interior Plains in western Canada are one of the three largest stores of organic carbon found in peatlands within the permafrost zone, the other two being the Hudson Bay Lowlands and the West Siberian Lowlands (Hugelius et al., 2020; Olefeldt et al., 2021). Within the sporadic and discontinuous permafrost zone of our study region >15% of the total peat plateau area has thawed and formed thermokarst bogs in the last 30 years (Baltzer et al., 2014; Gibson et al., 2018). Projections for this area suggests total permafrost lost from plateaus by 2050 (Chasmer and Hopkins, 2017).

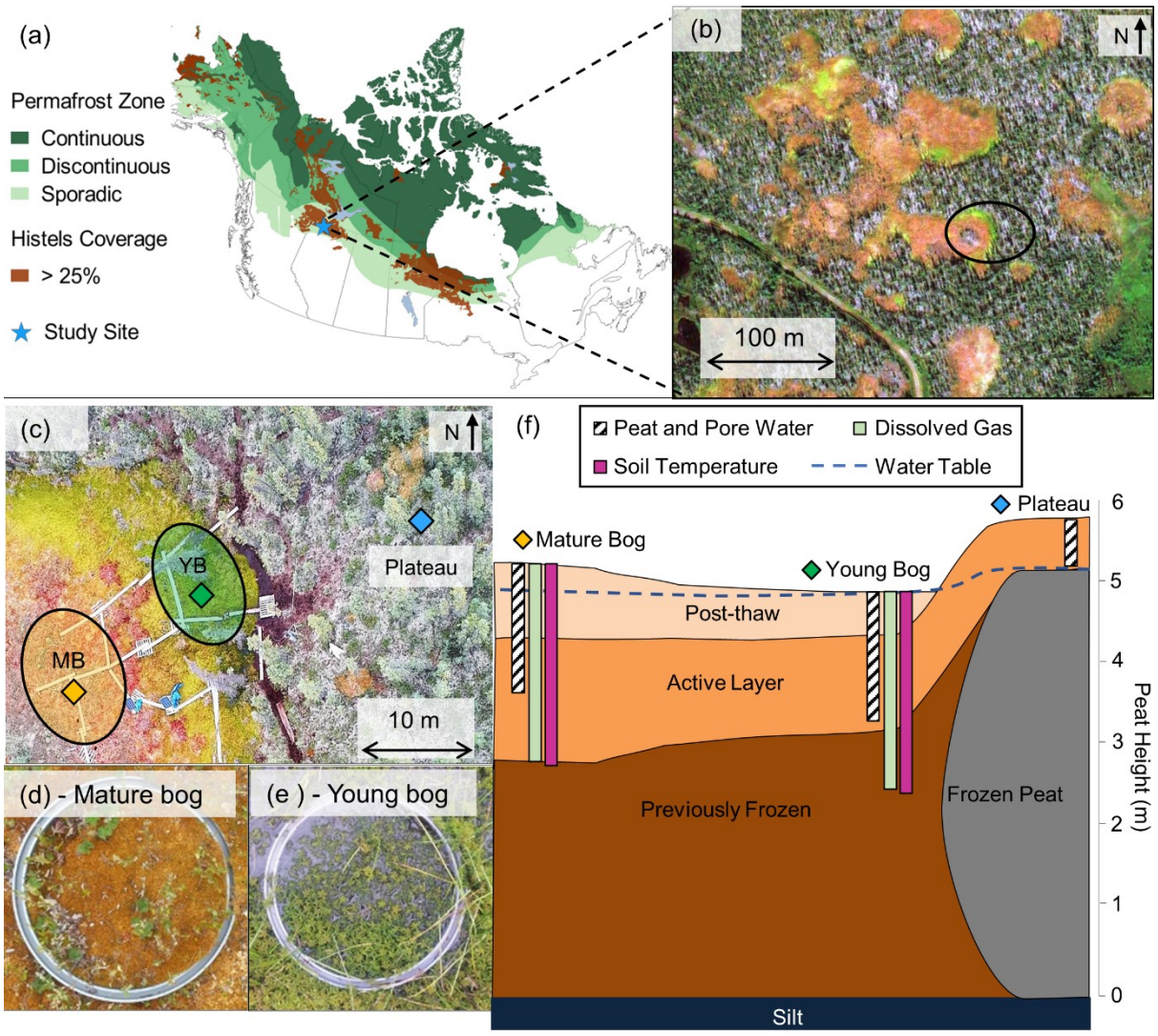

**Figure 1.** Lutose peatland site location and study design. (a) Site location (Lutose, Alberta, Canada 59.5°N, 117.2°W) in boreal western Canada. Green shading represents permafrost zonation (Brown et al., 1997) and brown shading represents areas with >25% permafrost peatland (histels) extent (Hugelius et al., 2014). (b) Geoeye satellite image of study site (image from https://zoom.earth/), 0.46 m resolution. Circle represents the area where sampling took place. (c) Aerial image of study transect, locations of peat and dissolved gas sampling in the plateau (blue diamond), young bog (green diamond), and mature bog (orange diamond), and area where collars for gas flux measurements were located in the young bog (YB, green) and mature bog (MB, orange) (Aerial photo credit: Olefeldt, David). (d, e) Surface vegetation in the mature bog and young bog (f) Soil profile of thaw transect based on (Heffernan et al., 2020). The transition to Post-thaw peat occurs at 29 cm and 71 cm in the young bog and mature bog respectively. Peat (core) and pore water (pore water peepers), including microbial community, sampling depth profile 0 – 160 cm shown as white column with diagonal black lines. Dissolved gas (diffusive samplers) sampling depth profile 0 – 245 cm shown as light green column. Soil temperature depth profile 0 – 250 cm shown as purple column. Average water table depth shown as dashed blue line.

The studied transect represents a space-for-time gradient of permafrost thaw that includes three thaw stages: a permafrost peat plateau, and a young (~30 years since thaw) and mature (~200 years since thaw) part of an adjacent thermokarst bog. The timing of permafrost thaw was previously determined by $^{14}C$ dating the shift in macrofossil vegetation indicative of thaw, at 29 cm in the young bog and at 71 cm in the mature bog (Figure 1f) (Heffernan et al., 2020). The peat plateau has an active layer thickness of ~70 cm and its surface is raised 1 – 2 m above the adjacent thermokarst bog due to the presence of excess ground ice, resulting in relatively dry surface conditions where the water table generally follows the deepening of the seasonally thawed peat layer (Zoltai, 1972). This thaw stage is characterized by a stunted, open black spruce (*Picea mariana*) canopy and ground cover of lichens (*Cladonia* spp.), *Sphagnum fuscum* hummocks, and low-lying ericaceous shrubs as is characteristic of the peat plateaus in the area (Vitt et al., 1994). The young bog stage is narrow (<5 – 10 m wide) and is located next to the actively thawing area of the peat plateau. The young bog has an average growing season water table position of 1.3 ± 4.9 cm below the peat surface. These inundated conditions result in the dominance of a hydrophilic vegetation community (Figure 1e) consisting of *Sphagnum riparium*, bog-sedge (*Carex limosa*), and rannoch rush (*Scheuchzeria*

*palustris*). The mature bog is ~10 – 15 m from the young bog and is drier, compared to the young bog, with an average growing season water table position of 22.9 ± 9.3 cm below the surface. The dominant vegetation reflects these drier conditions and consists of *Sphagnum fuscum, Sphagnum magellanicum,* leather leaf (*Chamaedaphne calyculata),* cloudberry *(Rubus chamaemorus), Eriophorum vaginatum* tussocks, and some black spruce (*Picea mariana)* regrowth (Figure 1d). The mature bog is located >10 – 20 m from the thawing plateau edge.

### *2.2 Site Preparation and Monitoring of Environmental Conditions*

The Lutose peatland study site was established in 2015 and a boardwalk was constructed to minimize disturbances along the peat plateau - thermokarst bog transect. Three collars for surface greenhouse gas flux (39 cm diameter) measurements were permanently installed to a depth of 20 cm in both the young and mature thermokarst bog stages. The top of each collar was aligned with the peat surface. PVC wells (2 cm diameter) were installed directly next to each collar and were used to manually monitor the water table position during each gas flux measurement. We monitored soil temperature (°C) at 10, 30, 50, 75, 100, 150, 200, and 250 cm every 30 min from May – September 2018 using permanently installed loggers (Hobo 8k Pendant Onset Computer, Bourne, MA, USA) in both thermokarst bog stages. Temperature depth profiles were established centrally among collars in each thermokarst bog stage, in areas that had similar vegetation, water table position, and distance from the thawing edge as the collars.

Custom made plexiglass pore water suction (Heffernan et al., 2021) and diffusive equilibration gas sampling devices (Knorr et al., 2009) were installed in July 2016 in the young and mature bog. These devices were installed in both thermokarst bog stages ~1 m from the nearest flux measurement collar. Pore water suction devices were installed to a

depth of 160 cm and consisted of 15 sampling depths, with each sampling depth connected to the surface via silicone tubing. This allowed for repeated non-destructive pore water sampling. Three diffusive gas sampling devices were installed in each thermokarst bog stage, where two collected dissolved soil gas samples from 5 – 95 cm deep and a third from 115 – 245 cm. Each diffusive gas sampler consisted of a PVC pipe with a 10 cm long sampling section centred at each sampling depth. Sampling sections consisted of ~2 m of silicon tubing (3 mm i.d., 5 mm o.d.) wrapped around the PVC pipe and kept in place by PVC-spacers at the top and bottom of each interval. Silicone tubes were sealed at one end whereas the other end was connected to polyurethane tubing (1.8 mm i.d.) that ran back up inside the PVC tube to reach the peat surface where it was sealed with a three-way stopcock. Silicone tubing has been shown to be permeable to gases such as $CO_2$ and $CH_4$ within a number of hours, while remaining impermeable to water, making it suitable for sampling of dissolved soil gases (Kammann et al., 2001).

### *2.3 Pore water chemistry and peat enzyme activity*

Pore water dissolved organic matter (DOM) chemistry and peat enzyme activity presented in this study have previously been published (Heffernan et al., 2021), and are briefly described here. Pore water samples for DOM chemistry were taken monthly from May – September 2018 using the previously described pore water suction devices in the young bog and mature bog. Three 60 mL samples were taken from all 15 measurement depths by applying a vacuum at the surface and collecting water with syringes via a three-way stopcock. Each water sample was immediately filtered through 0.7 µm pore size glass fiber filters (GF/F Whatman) into two acid-washed amber glass bottles, with one sample acidified with 0.6 mL 2N HCl to prevent further microbial activity. Pore water samples were transported in a cooled container and stored at 4 °C prior to analysis. Pore water DOM was

analyzed for pH, phosphate ($PO_4^{3-}$; µg $L^{-1}$), dissolved organic carbon (DOC; mg $L^{-1}$), total dissolved nitrogen (TDN; mg $L^{-1}$) concentrations, phenolic contents, specific UV absorbance at 254 nm (SUVA, L mg $C^{-1}$ $m^{-1}$; Weishaar et al., 2003) and spectral slope between 250 – 465 nm ($S_{250-465}$, $nm^{-1}$; Helms et al., 2008). SUVA and $S_{250-465}$ values are used to indicate aromaticity, with high SUVA indicating a high aromatic content and lower $S_{250-465}$ indicating low molecular weight and decreasing aromaticity (Hansen et al., 2016).

Peat cores extracted to a depth of 160 cm were stored at 4 °C for less than one week in the laboratory before homogenization to determine potential soil enzyme activities. We performed hydrolytic enzyme assays for four enzymes; phosphatase, β-N-glucosaminidase, β-glucosidase, and β-cellobiosidase using fluorogenic 4-methylumbelliferone labelled substrates (Dunn et al., 2014). We assayed oxidative enzyme activity by measuring laccase activity using syringaldazine (Criquet et al., 2000; Jassey et al., 2012). We summarized the activity of all enzymes using a multi-functionality index based on *z*-scores (Allan et al., 2015; Heffernan et al., 2021).

### *2.4 Surface Land-Atmosphere Gas Fluxes*

We measured surface land-atmosphere greenhouse gas fluxes ($CH_4$ and carbon dioxide; $CO_2$) monthly from May – September 2018 at the 3 collars in each peatland stage using the static chamber method (Carroll & Crill, 1997). The chamber used to capture land-atmosphere fluxes was a transparent cylindrical Plexiglass chamber with a basal area of 0.12 $m^2$, height of 0.40 m, and volume of 47.8 L. The chamber was equipped with three fans (Micronel Ventilator D341T012GK-2, BEDEK GmbH, Dinkelsbühl, Germany) to mix air during measurements and a temperature sensor (Hobo RH Smart Sensor, S-THB-M002, Onset computers, Bourne, USA) that was shaded from direct sunlight (Burger et al., 2016). An airtight seal was formed between the chamber and collar by pouring water in a ~1.5 cm deep well around the upper circumference of each collar. Land-atmosphere fluxes of $CO_2$

289 (ecosystem respiration) and $CH_4$ were captured simultaneously in darkened conditions by
290 covering the chamber with a reflective shroud. Gas concentrations were determined at a
291 temporal resolution of 1 s using an Ultraportable Greenhouse Gas Analyser (Los Gatos
292 Research, CA, USA) and real-time fluxes were monitored using the VNV® Viewer
293 (RealVNC® Limited, UK) application with an iPad mini 2 (Apple Inc.).

294 The rates of $CH_4$ and $CO_2$ land-atmosphere fluxes (*Flux*) were calculated using the ideal
295 gas law following:

296 $$Flux = slope\frac{P.V}{R.T.A} \quad (1)$$

297 where slope is the linear rate of change of gas concentration (μmol $mol^{-1}$ $second^{-1}$) over the
298 measurement period inside the chamber; P is an atmospheric pressure (atm) constant of 0.96
299 atm; V is chamber volume (L); R is the universal gas constant (L atm $K^{-1}$ $mol^{-1}$); T is the
300 average temperature (K) inside the chamber during the measurement; and A is the chamber
301 basal area ($m^2$). Chamber closure for each flux measurement was 5 minutes with the first 2
302 minutes discarded to ensure fluxes (i.e., change in concentration over time) with $R^2 > 0.75$.
303 We report $CO_2$ fluxes in g $CO_2$ $m^{-2}$ $day^{-1}$ and $CH_4$ fluxes in mg $CH_4$ $m^{-2}$ $day^{-1}$, with positive
304 values indicating fluxes to the atmosphere. To quantify the proportion of C being emitted as
305 $CH_4$, we standardized our $CO_2$ and $CH_4$ fluxes per g C emitted. The proportion of C emitted
306 as $CH_4$ ($CH_4$:C emissions) was calculated as

307 $$CH_4{:}\,C\ emissions = \frac{CH_4\ m^{-2}\ day^{-1}}{CH_4\ m^{-2}\ day^{-1} + CO_2\ m^{-2}\ day^{-1}} \quad (2)$$

308 *2.5 $\delta^{13}C$-signature of $CH_4$ emissions*

309 We assessed the $\delta^{13}C$-$CO_2$ and $\delta^{13}C$-$CH_4$ signatures of ecosystem respiration ($CO_2$) and
310 $CH_4$ emissions. This was done similarly to regular measurements of $CO_2$ and $CH_4$ fluxes, but
311 using a smaller, opaque chamber of 31.1 L and discrete syringe-samples for $\delta^{13}C$ analysis in

312 combination with the continuous monitoring of gas concentrations described above. Gas
313 syringe samples were taken using a 20 mL syringe via a three-way stopcock placed between
314 the sealed chamber and gas inlet port on the Ultraportable Greenhouse Gas Analyser. Gas
315 samples were then injected into a 37.5 mL sealed glass-vial that had been flushed with
316 nitrogen gas prior to sealing. Chamber enclosure time ranged from 30 – 50 minutes with 4 – 5
317 samples being taken during this time. Samples were taken either every 10-minutes or once a
318 minimum change in $CO_2$ (30 μmol $mol^{-1}$) and $CH_4$ (1 μmol $mol^{-1}$) concentrations was
319 observed. An atmospheric gas sample was used as a time-zero measurement when assessing
320 the change in concentration over time. Glass-vials containing samples were stored at 4 °C
321 until analysis. These measurements were taken in September and October 2016 from 1 collar
322 in both the young and mature bog, with each collar measured twice.
323 We measured the $\delta^{13}C$ values of gas samples from both the chamber fluxes and
324 atmospheric background. To assess whether the gas concentration of each sample fit within
325 the measurement range required for $\delta^{13}C$ analysis we measured $CO_2$ and $CH_4$ concentrations
326 using 1 – 3 mL from each vial. Following these concentration measurements, the remaining
327 sample (17 – 19 ml) was diluted with nitrogen gas to a final volume of 20 mL and injected
328 into a Small Sample Introduction Module (SSIM, Picarro, California, USA) system to
329 measure $\delta^{13}C$ signatures. The $\delta^{13}C$-$CO_2$ and $\delta^{13}C$-$CH_4$ signature was measured in-line with a
330 cavity ring-down spectrometer (G2201-L, Picarro, California, USA) that had been calibrated
331 using certified standards.
332 We then used the time-series of $\delta^{13}C$-$CH_4$ and $CH_4$ concentrations to estimate the $\delta^{13}C$-
333 $CH_4$ signature of the $CH_4$ released to the atmosphere using Keeling plots (Keeling, 1958).
334 Using this approach, the $\delta^{13}C$-$CH_4$ signature of gas in each sample is plotted on the *y*-axis
335 against the inverse of $CH_4$ gas concentrations ($1/[CH_4]$). The *y*-axis intercept of the linear
336 regression represents the mean isotopic signature of the $CH_4$ source (Fisher et al., 2017).

While fractionation during diffusive transport may influence these estimates, it has been shown in similar systems to be of minor importance compared to other contributing processes (Preuss et al., 2013; Nielsen et al., 2019).

### *2.6 Dissolved gas depth profiles*

Dissolved gas samples were collected using diffusive equilibration gas sampling devices. Samples were taken from the following 15 depths: every 10 cm down to 95 cm starting at 5 – 15 cm, and then at 115 cm, 140 cm, 165 cm, 195 cm, and 245 cm. Once a month from May – September 2018 a ~7 mL gas sample was drawn from each depth using a 10 mL plastic syringe. These gas samples were immediately injected into a 10 mL sealed glass-vial that had been flushed with nitrogen gas prior to sealing, and then were stored at 4 °C until analysis. A total of 214 $CO_2$ and 211 $CH_4$ dissolved gas concentration measurements were made by injecting 1 – 3 mL of gas into a gas chromatograph with an FID and $CO_2$ methanizer (8610C Gas Chromatograph, SRI Instruments, California, USA). We measured $\delta^{13}C\text{-}CO_2$ and $\delta^{13}C\text{-}CH_4$ signatures using the previously mentioned cavity ringdown spectrometer and SSIM system. As with surface chamber gas samples, dissolved gas samples were diluted with $N_2$ to 20 ml. However, dissolved gas concentrations were considerably higher than gas concentrations found in the surface chambers, and some were well above the optimal concentration range required for accurate $\delta^{13}C$ analysis for the SSIM system even after dilution. To fit within measurement range of the system, further dilution resulted in $CO_2$ concentrations below detectable limits. As such, we were able to obtain 90 and 75 measurements of $\delta^{13}C\text{-}CH_4$ in the young and mature bog, respectively, and 93 measurements of $\delta^{13}C\text{-}CO_2$ in both.

We used the $\delta^{13}C\text{-}CO_2$ and $\delta^{13}C\text{-}CH_4$ signature of each gas sample to calculate the apparent fraction factor $\alpha_c$, where $\alpha_c = [^{13}C\text{-}CO_2 + 1000]/[^{13}C\text{-}CH_4 + 1000]$. The $\alpha_c$ can serve

as an isotopic indicator of the pathway of methanogenesis, with typical values of 1.060 – 1.090 observed for hydrogenotrophic methanogenesis and 1.040 – 1.060 for acetoclastic methanogenesis (Chanton et al., 2005).

### *2.7 Peat and pore water sample collection for microbial community composition analyses*

Microbial community composition was characterized in both peat and peat pore water samples from depths between 0 – 160 cm in the young bog and mature bog. Focusing on peat samples, microbial community composition in the active layer of the peat plateau was assessed from depths between 0 – 30 cm. Peat cores were extracted in June and September 2018. Near-surface cores were extracted using a cutting tool to 30 cm deep in the peat plateau and young bog, and 50 cm deep in the mature bog. Surface cores were limited to 30 cm in the plateau due to the presence of ground ice during sampling in June. Surface core depths differed between the young bog and mature bog due to differences in the water table position. Deeper core sections (down to 160 cm) in the young bog and mature bog were extracted using a Russian peat corer (4.5 cm inner-diameter, Eijkelkamp, Giesbeek, The Netherlands). Cores were extracted from two boreholes located ~20 cm apart, alternating between boreholes to avoid disturbance contamination from the 10 cm corer tip during the coring process. To do so, 50 cm long core sections were taken alternatively from each borehole, with each core having a 10 cm overlap with the previous core taken from the adjacent borehole. In the field, immediately after the entire core was extracted, cores were divided into 15 subsections. The first two subsections contained peat from 0 – 5 cm and 5 – 10 cm, followed by 10 cm increments down to 120 cm, and two further subsections from 130 – 140 cm and 150 – 160 cm. Peat from each interval was sub-sampled using sterilized forceps and placed directly into Whirl-Pak® bags, and frozen within 3 hours of sampling for transportation back

385 to the laboratory. Once samples reached the laboratory, they were frozen at -80 °C until
386 analysis.

387 We also sampled peat pore water at all 15 peat sampling depths in September 2018 from
388 the pre-installed pore water suction sampling devices mentioned above. We extracted 60 mL
389 pore water samples by applying a vacuum at the surface and collecting water with new plastic
390 60 mL syringes. Pore water was immediately filtered through sterile 0.2 μM pore size
391 Polyvinylidene difluoride (PVDF) membrane sterivex filters (MilliporeSigma). Microbial
392 cells were retained on the filter, and remaining porewater in the sterivex was removed via
393 extrusion using a 60 mL sterile syringe. Sterivex filters were then immediately flash-frozen at
394 -80 °C in a liquid nitrogen dry-shipper to preserve microbial community members until
395 analysis could take place.

396 *2.8 DNA extraction*

397 Genomic DNA was extracted from all peat and pore water samples using the DNeasy
398 PowerSoil kit (Qiagen) and the PowerWater DNeasy kit (Qiagen), respectively, to assess the
399 differences in microbial community structure. Extraction of DNA from both sample types
400 was followed as described by the manufacturer (Qiagen), with two modifications: (i) for peat
401 samples, prior to mechanical lysis using bead beating, the prepared samples were chemically
402 lysed by incubation at 70 °C for 10 minutes in the provided lysis solution, and (ii) sterivex
403 (pore water) samples were incubated with rotation at 37 °C following addition of lysis buffer.
404 These modifications were made to increase total DNA yield. The amount of isolated DNA
405 from each sample was then determined using a Qubit fluorometer (model 2.0, using the 1×HS
406 dsDNA kit), with concentrations ranging between ~0.1 and 22.4 ng $\mu L^{-1}$. This extracted DNA
407 served as the template for polymerase chain reaction (PCR) analyses described below.

408 2.9 *Sequencing and computational analyses*

We amplified 16S rRNA genes using universal prokaryotic primers 515F (Parada, Needham & Fuhrman, 2016) and 926R (Quince et al., 2011). Each primer also contained a six-base index sequence for sample multiplexing (Bartram et al., 2011). The PCR mix (25μL total volume) contained 1 × Q5 reaction buffer, 0.5 μM forward primer, 0.5 μM reverse primer, 200 μM dNTPs, 0.500 U Q5 polymerase (New England Biolabs, Ipswich,M.A, U.S.A) and 2.5 μL of genomic template. Genomic extracts with DNA concentrations of greater than 2 ng $\mu L^{-1}$ were diluted 1:100 in nuclease-free water. The PCR was performed as follows: 95 °C for 3 minutes, 35 cycles of 95 °C for 30 seconds, 60 °C for 30 seconds, 70 °C for 1 minute and a final extension of 70 °C for 10 minutes. Pooled 16S rRNA gene amplicons were purified using Nucleomag beads and a 4.5 pM library containing 50% PhiX Control v3 (Illumina, Canada Inc., NB, Canada) was sequenced on a MiSeq instrument (Illumina Inc., CA, USA) using a 2 × 250 cycle MiSeq Reagent Kit v3 (Illumina Canada Inc) at the Molecular Biology Service Unit (MBSU, University of Alberta). The MiSeq reads were demultiplexed using MiSeq Reporter software version 2.5.0.5. Each read pair was assembled using the paired-end assembler for Illumina sequences (PANDAseq; Masella, Bartram & Truszkowski, 2012) with a quality threshold of 0.9, dictating that 90% of overlapping reverse and forward reads must match in order to assemble reads into read pairs. Assembled reads were analyzed using the Quantitative Insights Into Microbial Ecology II pipeline (QIIME2; Boylen et al., 2020). Sequences were clustered into amplicon sequence variants (ASVs) with chimeric sequences, singletons and low abundance ASVs removed using DADA2 (Callahan et al., 2019). All representative sequences were classified with the Greengenes reference database, using the most recent release (version 13.8; McDonald et al., 2012). Although Greengenes is not updated as frequently as the SILVA database, we chose to use it to classify our ASVs as a comparison of both databases revealed that they captured a similar number of archaea (total of 51187 methanogenic read counts attributed to SILVA *versus* 51141

methanogenic read counts attributed to Greengenes). The taxonomic resolution between both databases was also similar, identifying the same kinds of phyla, families and genus, and methanogens (e.g., methanoregula, methanosarcinales, etc.). Given these similarities, and the fact that methanogen nomenclature has not changed significantly over time, we ultimately chose to use Greengenes because it was able to resolve more methanogenic families belonging to Methanocelalles and Methanomassiliicoccaceae particularly, compared to SILVA. The Greengenes database is also still commonly used to explore methanogenic archaeal communities in current literature (Vanwonterghem et al., 2016, Lin et al., 2017, Carson et al., 2019). Furthermore, since 1021 methanogenic reads were captured per sample, on average, using Greengenes and are comparable to other studies (Vishnivetskaya et al., 2018; Holm, et al., 2020) we believe that our approach is sufficient for covering methanogen diversity.

### *2.10 Statistical analyses*

All statistical analyses were carried out in R (Version 3.4.4, R Core Team, 2015) using the *nlme*, *vegan*, *factoextra*, *ggplot2*, *VariancePartition* and *ggpubr* packages (Pinheiro et al., 2017; Oksanen et al., 2013; Kassambara & Mundt, 2017; Wickham, 2016; Hoffman & Schadt, 2016; Kassambara, 2018). For Analysis of Variance (ANOVAs), distribution of the data was inspected visually for normality along with the Shapiro-Wilk test. We tested homogeneity of variances using the *car* package and Levene's test (Fox and Weisberg, 2011). We report uncertainty as ± 1 standard deviation, except for land-atmosphere greenhouse gas fluxes which we report as ± 95% confidence intervals. We here define the statistical significance level at 5%.

We used ANOVAs and Bonferroni post-hoc tests on linear mixed effects models to address our second hypothesis and to evaluate significant differences and seasonal trends in

458 greenhouse gas fluxes and dissolved gas depth profiles. We performed these tests to assess
459 whether thaw stage (young bog or mature bog) influenced greenhouse gas fluxes and
460 dissolved gas depth profiles. This approach was used to test for significant differences in $CH_4$
461 fluxes, ratio of $CH_4$:C emissions, and source $^{13}C$-$CH_4$ signature intercepts of Keeling plots
462 between young bog and mature bog stages. In each linear mixed effect model, sampling
463 month and peatland stage were defined as fixed effects whereas sampling collar was defined
464 as a random effect. Similarly, we tested for significant differences between the young and
465 mature bog depth profiles with respect to dissolved $CH_4$ and $CO_2$ concentrations, $\delta^{13}C$-$CH_4$
466 and $\delta^{13}C$-$CO_2$ values, $\alpha_c$ values, and pore water chemistry. In these models, sampling month
467 and peatland stage were defined as fixed effects while sample depth was defined as a random
468 effect.

469 Following microbial 16S rRNA gene sequencing, sample reads were rarefied to the
470 lowest read count of 28,129 for all subsequent analyses. These sequences represent whole
471 microbial community data that was used to determine whether there was evidence of changes
472 in microbial community structure representing the successional peatland stages following
473 permafrost thaw throughout the 160 cm depth peat profile. In addition, to address our first
474 hypothesis, we assessed differences in community composition across both peat and pore
475 water and to determine whether seasonality impacted microbial community structure in both
476 sample matrices. Here, Bray Curtis dissimilarity matrices for overall microbial community
477 data were used, at 999 permutations, to identify distinct groupings assessed at the 95%
478 confidence interval in NMDS ordinations. These distinct groupings were further evaluated for
479 significance using the non-parametric permutational analysis of variance (PERMANOVA)
480 test.

481 To further test our first hypothesis, methanogens were selected at the order level from
482 our whole community data using Greengenes-assigned taxonomy. Utilizing their assigned

taxonomy, the pathways through which identified methanogens conduct methanogenesis was determined by comparing our findings with the literature (Berghuis et al., 2019; Stams et al, 2019; Kendall & Boone, 2006; Zhang et al., 2020). Focusing on the methanogenic community allowed us to specifically assess how permafrost thaw affects the microbial community responsible for $CH_4$ production and net $CH_4$ emissions following thaw. We utilized our methanogenic community data to construct redundancy analyses (RDA) and relative abundance bar plots. RDAs were conducted using a Hellinger-transformed methanogenic community. Explanatory variables (i.e., dissolved concentrations of $CO_2$, $CH_4$, DOC, temperature, enzymatic activity estimate, thaw stage, depth, and distance to water table) were scaled about the mean. These explanatory variables had variance standardized, were checked for collinearity (parameters with variance inflation value > 10 were removed) and selected for significance using backward selection, set at 1,000 permutations. The significance of the RDA model, and of each axis was tested using ANOVAs, set at 999 permutations. Variance partitioning analyses were conducted to assess the contribution of significant environmental parameters (i.e., thaw stage and distance to water table) on the structuring of the Hellinger-transformed methanogenic community. Distance from water table reflects the distance (in cm) a certain sample is from the water table in different stages of thaw (young bog and mature bog). Due to the smaller size of our methanogenic community relative to the total community, and the lack of some data at certain depths, we combined pore water and peat samples together for these analyses. Relative abundance, which measures how common or rare a particular microorganism is relative to the entire microbial community, of methanogenic orders related to acetoclastic or hydrogenotrophic methanogenesis processes were plotted according to depth. Significant differences in methanogenic community composition between depths were assessed using the non-

parametric Kruskall-Wallis test with a Benjamini-Hochberg correction for multiple comparisons, after running a Wilcox rank sum test.

## 3. Results

### *3.1 Site environmental conditions*

The young bog was wetter and warmer than the mature bog throughout the May – September 2018 study period. In June, following snowmelt, the water table was at its highest at 2.2 ± 0.6 cm above the surface in the young bog. The highest water table position in the mature bog was 17.5 ± 1.9 cm below the peat surface and observed in July. The water table dropped during the season and in September was 5.7 ± 2.2 cm and 27.3 ± 1.2 cm below the peat surface, in the young bog and mature bog respectively. In the plateau, the seasonally thawed layer gradually deepened during the growing season, with an active layer depth of 79.5 ± 13.7 cm measured in September. The water table in the peat plateau followed the deepening of the seasonally thawed layer.

Soil temperatures followed the seasonal climate but were dampened and had temporal lags in deeper peat layers (Figure S1a). The highest young bog and mature bog soil temperatures at 10 cm depth occurred in July, at 14.3 and 14.1 °C, respectively. At 100 cm depth the maximum temperatures occurred in August and September, at 8.6 and 6.9 °C, respectively for the young and mature bog. Soil temperatures at 250 cm were still rising at the end of September, peaking at 4.1 and 3.2 °C in the young bog and mature, respectively. The young bog was consistently warmer than the mature bog throughout the study by on average 0.9 ± 0.9 °C, 1.8 ± 1.0 °C, and 0.5 ± 0.4 °C at 10 cm, 100 cm, and 250 cm depths, respectively.

Across all depths and sampling occasions, average pH was higher (ANOVA: $F_{(1, 77)} = 35.2$, $P < 0.001$) in the young bog than in the mature bog at 4.1 ± 0.2 and 3.9 ± 0.2

531 respectively. In contrast, DOC at 69.2 ± 18.4 and 53.8 ± 5.4 mg C $L^{-1}$ (ANOVA: $F_{(1, 82)}$ =
532 38.7, $P < 0.001$) and total dissolved nitrogen at 1.5 ± 1.4 and 0.9 ± 0.1 mg $L^{-1}$ (ANOVA: $F_{(1,}$
533 $_{82)}$ = 12.8, $P < 0.01$) were higher in the mature bog than in the young bog, respectively.
534 Average SUVA values were higher (ANOVA: $F_{(1, 82)} = 103.5$, $P < 0.001$) in the young bog
535 (3.2 ± 0.4 L mg $C^{-1}$ $m^{-1}$) compared to the mature bog (2.6 ± 0.4 L mg $C^{-1}$ $m^{-1}$), indicating
536 DOM with a greater aromatic content in the young bog. However, average spectral slope
537 ($S_{250-465}$) values were also greater (ANOVA: $F_{(1, 81)} = 6.9$, $P < 0.05$) in the young bog (-
538 0.016 ± 0.002 $nm^{-1}$) compared to the mature bog (-0.017 ± 0.003 $nm^{-1}$), indicating lower
539 molecular weight and decreasing aromaticity. Average phenolics (0.6 ± 0.2 and 0.6 ± 0.2 mg
540 $L^{-1}$) and phosphate ($PO_4^{3-}$: 9.0 ± 14.3 and 6.7± 3.0 µg $L^{-1}$) were similar between the young
541 bog and mature bog, respectively, across all depths and sampling occasions. Full details of
542 DOM chemistry results can be found in Heffernan et al., (2021). Of note is the fact that the
543 pore water chemistry was compared across all depths in this study, in contrast to Heffernan et
544 al., (2021) in which pore water found above and below the transition indicating permafrost
545 thaw was compared.

546 *3.2 Concentrations and isotopic signatures of dissolved gases*

547 Dissolved $CH_4$ increased with depth below the water table in both the young and
548 mature bog (Figure 2a). Dissolved $CH_4$ concentrations in the young bog increased with depth,
549 from19 µmol $L^{-1}$ at 5 cm depth, to a peak of 5,400 µmol $L^{-1}$ at 195 cm. Dissolved $CH_4$
550 concentrations in the mature bog remained low above the water table (<6 µmol $L^{-1}$ below 25
551 cm), but then increased to 4,100 ± 1,700 µmol $L^{-1}$ between 115 and 250 cm depth and peaked
552 at 6,800 µmol $L^{-1}$. Dissolved $CO_2$ concentrations followed a very similar pattern to $CH_4$,
553 increasing with depth in both the young and mature bog (Figure 2b). Again, the mature bog
554 had overall higher concentrations, with mean average values ranging from 340 – 1,295 µmol

555 $L^{-1}$ and peaking at 1,500 µmol $L^{-1}$ at 85 cm. Whereas in the young bog average values ranged

556 from 113 – 960 µmol $L^{-1}$ and peaked at 1,200 µmol $L^{-1}$ at 95 cm (Figure 2b).

557

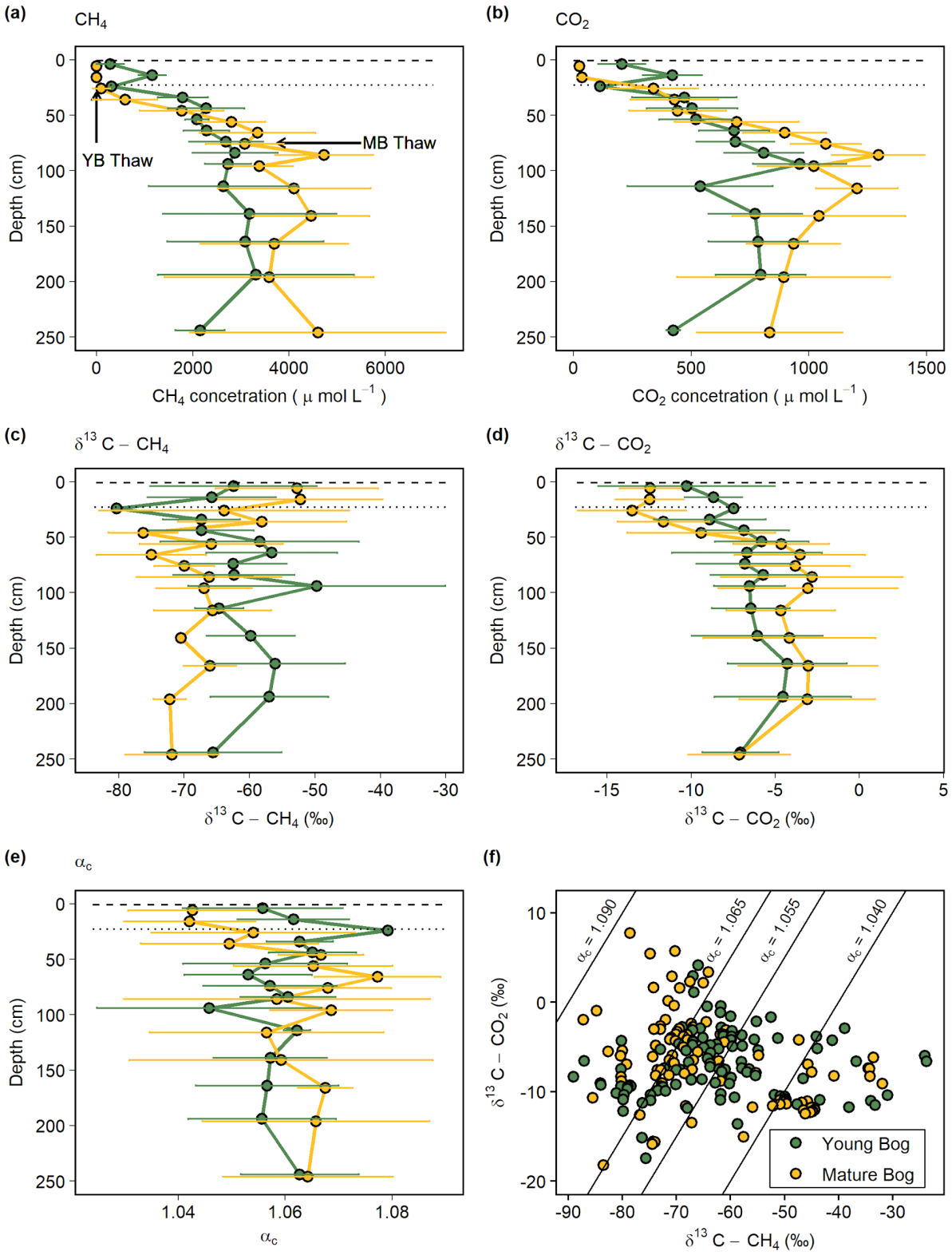


558

**Figure 2.** Average seasonal (May – September) depth profiles in the young (green, black circles) and mature (yellow, black circles) bog of (a) dissolved $CH_4$ concentration (μmol $L^{-1}$), (b) dissolved $CO_2$ concentration (μmol $L^{-1}$), (c) $\delta^{13}C$-$CH_4$ (‰), (d) $\delta^{13}C$-$CO_2$ (‰), and (e) apparent fractionation factor ($\alpha_c$) between dissolved $CH_4$ and $CO_2$. (f) Cross-plot of corresponding $\delta^{13}C$-$CH_4$ and $\delta^{13}C$-$CO_2$ values (‰) in the young bog and mature bog, from raw data used in panels (c) and (d). Diagonal lines represent different $\alpha_c$ where $\alpha_c$ 1.040 – 1.065 represents acetoclastic methanogenesis, and $\alpha_c$ 1.055 – 1.09 represents hydrogenotrophic methanogenesis (Whiticar, 1999). (a) – (e) Dashed and dotted horizontal lines represent water table depth in the young (YB) and mature bog (MB) respectively. Arrows in panel (a) represent depth of thaw transition in both the young (29 cm) and mature bog (71 cm), i.e., the transition from deep peat (accumulated prior to thawing) and shallow peat (accumulated post thawing).

The young bog and mature bog had distinct profiles of $\delta^{13}C$ values for both $CH_4$ and $CO_2$ (Figure 2c, d). The young bog had no apparent trend with depth for both $\delta^{13}C$-$CH_4$ (ANOVA; $F_{(14, 45)} = 1.75$, $P = 0.08$) and $\delta^{13}C$-$CO_2$ (ANOVA; $F_{(14, 46)} = 1.79$, $P = 0.07$), averaging -62.4 ± 7.0 ‰ and -6.8 ± 1.6 ‰, respectively (Figure 2c, d). In the mature bog we observed significant depth trends for both $\delta^{13}C$-$CH_4$ (ANOVA: $F_{(14, 43)} = 3.19$, $P < 0.01$) and $\delta^{13}C$-$CO_2$ (ANOVA: $F_{(14, 49)} = 6.22$, $P < 0.001$). These significant depth trends are due to isotopically heavy $\delta^{13}C$-$CH_4$ and light $\delta^{13}C$-$CO_2$ above the water table, which suggests an influence from $CH_4$ oxidation. When comparing $\delta^{13}C$ depth profiles between the thermokarst bogs we focused on those values taken from under the water table to avoid the effect of $CH_4$ oxidation observed above the water table in the mature bog. Under the water table, $\delta^{13}C$-$CH_4$ values in the mature bog were significantly lighter (ANOVA: $F_{(1, 64)} = 18.72$, $P < 0.001$) compared to the young bog at an average of -68.7 ± 5.0 ‰ and -62.4 ± 7.0 ‰, respectively. Conversely, the mature bog had isotopically heavier $\delta^{13}C$-$CO_2$ than the young bog below the water table (ANOVA: $F_{(1, 71)} = 13.86$, $P < 0.001$).

The apparent fractionation factor ($\alpha_C$) is a robust parameter to characterize the relative contribution of $CH_4$ production pathways, with values of 1.040 – 1.060 indicating acetoclastic methanogenesis and 1.060 – 1.090 for hydrogenotrophic methanogenesis (Chanton et al., 2005). Similar to the gas $\delta^{13}C$ depth-profiles, we found no clear trend with

depth for $\alpha_C$ values in the young bog (ANOVA; $F_{(14, 44)} = 0.87$, $P = 0.59$) with an average of 1.058 ± 0.012 and range of 1.018 – 1.079 (Figure 2e). In the mature bog, we found a clear depth trend in $\alpha_C$ values (ANOVA: $F_{(14, 43)} = 5.71$, $P < 0.001$). Similar to the $\delta^{13}C$ depth profiles in the mature bog, this significant depth trend in $\alpha_C$ is due to the influence of $CH_4$ oxidation above the water table, with the lowest $\alpha_C$ values being those from samples collected above the water table at 5, 15, and 25 cm. The average $\alpha_C$ beneath the water table in the mature bog was 1.064 ± 0.017 and ranged from 1.015 – 1.094. When comparing $\alpha_C$ values from beneath the water table between the young and mature bog we found that $\alpha_C$ values were significantly lower in the young bog (ANOVA: $F_{(1, 63)} = 30.8$, $P < 0.001$).

In the isotopic ratio cross-plot of $\delta^{13}C$-$CH_4$ and $\delta^{13}C$-$CO_2$ (Figure 2f), most of the young bog had $\alpha_C$ values of between 1.055 – 1.065 (29 in total), with a greater number of samples (21) between $\alpha_C$ =1.040 – 1.055, compared to the mature bog (15). In contrast, a greater proportion of the mature bog samples had $\alpha_C > 1.065$ (42 in the young bog and 52 in the mature bog). There was no clear depth trend in the $\alpha_C$ values and no samples in this study had $\alpha_C > 1.090$. Several samples (13) from the young bog and mature bog had $\alpha_C$ values of < 1.040, likely due $CH_4$ oxidation (Knorr et al., 2009).

### *3.3 Magnitude and isotopic signature of land-atmosphere gas fluxes*

The young bog had almost three times greater average $CH_4$ fluxes than the mature bog during the May – September study period, at 82.3 ± 21.9 mg $CH_4$ $m^{-2}$ $day^{-1}$ and 30.8 ± 10.6 mg $CH_4$ $m^{-2}$ $day^{-1}$, respectively (Figure 3a). Fluxes of $CH_4$ in the young bog were greatest between June and August, ranging from 80.6 ± 40.3 mg $CH_4$ $m^{-2}$ $day^{-1}$ to 100.9 ± 63.1 mg $CH_4$ $m^{-2}$ $day^{-1}$. The lowest young bog $CH_4$ fluxes were observed in September at 55.0 ± 17.7 mg $CH_4$ $m^{-2}$ $day^{-1}$ (Figure S3a). Mature bog $CH_4$ fluxes were greatest in September (55.8 ± 21.1 mg $CH_4$ $m^{-2}$ day-1) and lowest in May (5.6 ± 2.7mg $CH_4$ $m^{-2}$ $day^{-1}$). Ecosystem

614 respiration ($CO_2$ emissions measured with dark chambers) was significantly lower in the
615 young bog than mature bog, with study period averages of 0.6 ± 0.3 and 1.9 ± 0.3 g $CO_2$ $m^{-2}$
616 $day^{-1}$, respectively (Figure S3). Maximum ecosystem respiration in the young bog occurred in
617 August (1.6 g $CO_2$ $m^{-2}$ $day^{-1}$) and was much lower during the other four months (monthly
618 averages of 0.2 to 0.4 g $CO_2$ $m^{-2}$ $day^{-1}$). Ecosystem respiration rates in the mature bog were
619 elevated from June to August (monthly averages between 2.1 and 2.6 g $CO_2$ $m^{-2}$ $day^{-1}$),
620 and decreased in September (0.8 g $CO_2$ $m^{-2}$ $day^{-1}$). The proportion of total C emissions (sum
621 of $CH_4$ and $CO_2$ emissions) released as $CH_4$ were an order of magnitude greater in the young
622 bog than mature bog stage, at 18 and 2% respectively. This was a result of both higher $CH_4$
623 emissions and lower ecosystem respiration (Figure S3) in the young bog. The $\delta^{13}C$-$CH_4$
624 signature of $CH_4$ emissions (intercept values from Keeling plots), in the young bog were
625 significantly greater than those observed in the mature bog (Figure 3c; ANOVA: $F_{(1, 4)}$ =
626 20.67, $P < 0.05$). The average $\delta^{13}C$-$CH_4$ signature of $CH_4$ emissions in the young bog (n = 4)
627 was -66.5 ± 1.4‰ (95% CI) and 78.5 ± 5.6‰ (95% CI; Figure 3c) in the mature bog
628 emissions (n = 4).

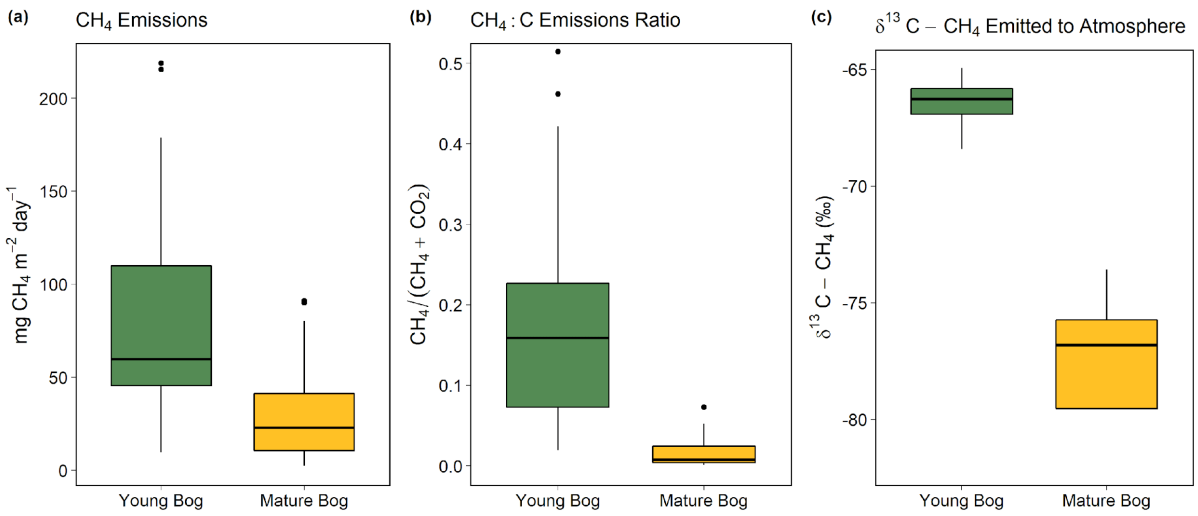


629

630 **Figure** 3. Magnitude and isotopic signature of greenhouse gas fluxes from the young bog
631 (green) and mature bog (yellow) shown as boxplots. Boxes represents the interquartile range
632 (25 – 75%), with median shown as black horizontal line. Whiskers extend to 1.5 times the
633 interquartile range (distance between first and third quartile) in each direction, with outlier

data plotted individually as black dots (a) The magnitude of net land-atmosphere $CH_4$ emissions as measured by soil chambers. (b) The ratio between $CH_4$ emissions and the sum of $CO_2$ emissions (ecosystem respiration) and $CH_4$, both standardized to per g C. (c) Intercept values of Keeling plots indicating the $\delta^{13}C$-$CH_4$ signature of $CH_4$ emissions. Isotopically heavier (i.e., less negative) $\delta^{13}C$-$CH_4$ is produced via acetoclastic methanogenesis, whereas isotopically lighter (i.e., more negative) $\delta^{13}C$-$CH_4$ is produced via hydrogenotrophic methanogenesis, The $CH_4$ and $CO_2$ land-atmosphere fluxes shown in (a) and (b) were measured once a month from May – September 2018. The $\delta^{13}C$-$CH_4$ of $CH_4$ emitted to the atmosphere was measured in September and October 2016 (see methods for details and Figure S4 for Keeling plots).

### *3.4 Microbial community structure along the permafrost peatland thaw gradient*

We used NMDS ordinations to assess differences in microbial community structure between solid peat and pore water samples, between sampling depths, and between the plateau, young bog, and mature bog. The only exception was the plateau, where only peat samples were collected (i.e., no pore water samples). Microbial community structure in peat was determined to be significantly different from porewater microbial communities (PERMANOVA, $R^2 = 0.13$, $P < 0.05$, Figure 4). The differences observed in the microbial community structure between peat and pore water samples could be a function of the different extraction methods used to extract DNA (Carrigg et al., 2007). Among the pore water samples, distinct microbial communities were found to be associated with the young bog and mature bog. Similarly, microbial community structure in peat was found to be significantly distinct between the three successional stages (plateau peat, young bog and mature bog; Figure 4; PERMANOVA, $R^2 = 0.18$, $P < 0.05$). There is also a common trend in vertical community structuring for all sample matrices according to depth. Changes in overall microbial community composition in both peat and pore water, across a vertical profile (to a maximum depth of 160 cm), illustrate a confluence in microbial community structure with depth in both the young and mature bog (Figure 4). In other words, community structure was most dissimilar at depths closer to the surface (Figure 4, Figure S2, c; PERMANOVA; $R^2 =$

0.16, $P < 0.05$). This trend was particularly evident in the porewater samples (Figure 4). In the peat samples, though microbial communities did not fully converge, deeper young bog peat (i.e., 90 – 160 cm) communities did become more similar to communities found in the mature bog at intermediate depths (i.e., 30 – 70 cm), based on the nearness of sample points on the NMDS (Figure 4). We also observed that the mature bog near-surface peat samples were located closer to the plateau peat on the NMDS (Figure 4, PERMANOVA, $R^2 = 0.4$, $P = 0.1$). It was not possible to assess the presence of this cyclic succession (from young bog to mature bog to plateau) in the pore water samples since we did not characterize the microbial community in the plateau pore water. Finally, we also assessed the effect of seasonality on microbial community structure and found no effect with regards to sampling month (PERMANOVA; $R^2 = 0.02$, $P = 0.090$).

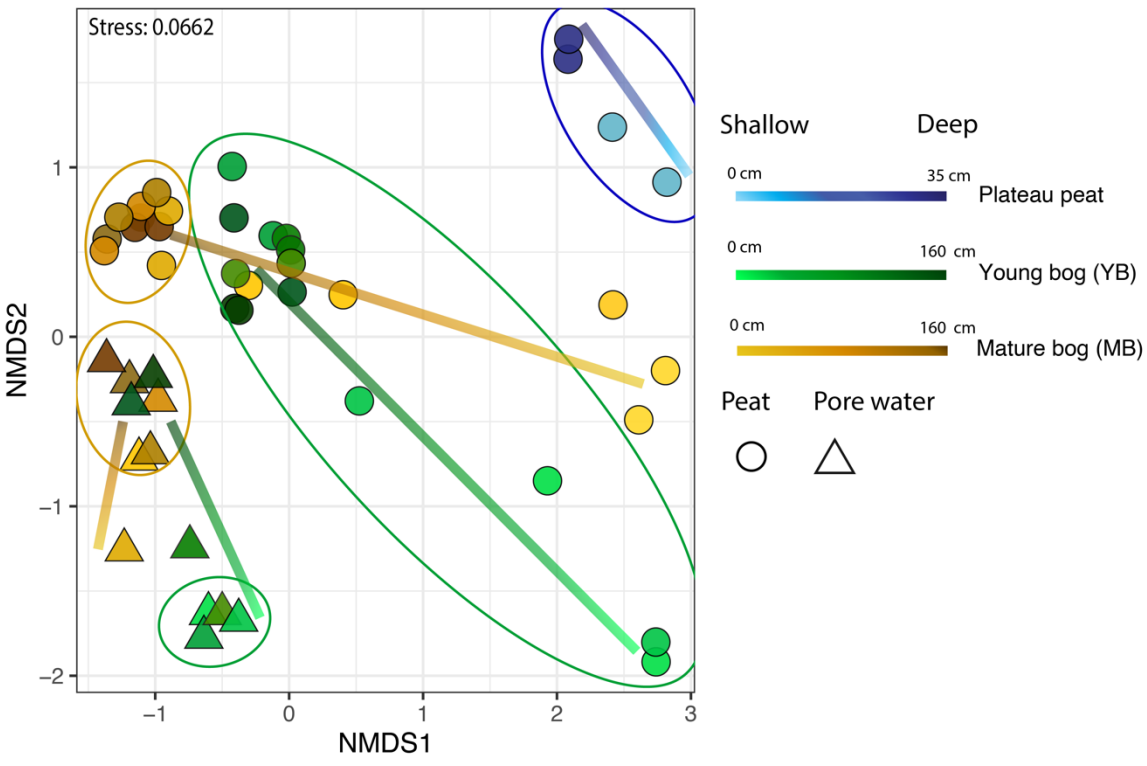


**Figure 4.** Microbial community distribution according to stage of peat/pore water. NMDS ordinations of amplicon sequencing variant (ASV) data demonstrate significant community dissimilarities (PERMANOVA, $R^2 = 0.13$, $P < 0.05$) according to thaw stage for both pore water (shown by the triangles) and peat (shown by the circles) samples, encircled by 95% confidence intervals. Colour gradient and lines demonstrate the shift in microbial community

structure along vertical depth profiles where lighter shades indicate samples closer to the surface.

The total archaeal community comprised 6% of the entire microbial dataset. Methanogen-related orders comprised 54% of this archaeal dataset and demonstrated marked differences in the relative abundance of acetoclastic-related methanogens according to thaw stage and depth in both peat and pore water samples (Figure 5; Figure S2). In the young and mature bog peat samples, hydrogenotrophic-related methanogens were ubiquitously present throughout both depth profiles (Figure 5a). In comparison, acetoclastic-related methanogens exhibited a relatively restricted presence, only present at specific depths (Figure 5a). These communities were most abundant (>25% of the total methanogenic community) near the surface in the young bog, just above and below the thaw transition zone (Figure 5a). In the pore water, hydrogenotrophic methanogens were also dominant throughout depths in both stages of thaw (Figure 5b). However, in contrast to peat samples, acetoclastic methanogens were virtually absent in the pore water, although minimally present (i.e., $\leq$ 10% relative abundance) at depths between 35 and 155 cm, all found below the thaw transition zone (Figure 5b).

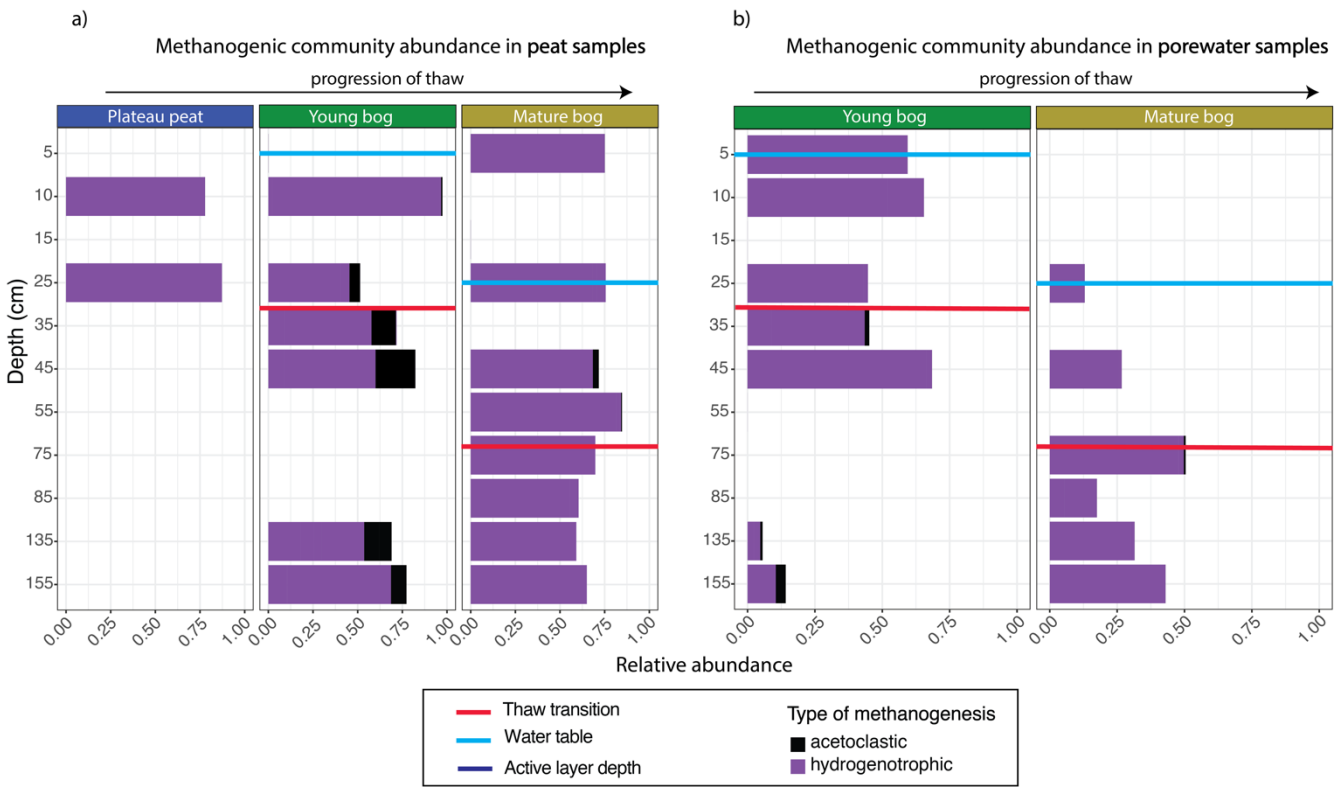

**Figure 5.** Relative abundance of archaeal orders according to putative methanogenic capability, along a depth profile for peat and pore water samples. Samples are arranged according to depth (y axis), with the relative abundance of methanogenic archaea resolved shown on the x axis. Note that the y axis does not uniformly progress in 10 cm increments. Progression of thaw is shown from plateau peat to young bog to mature bog at the top of the figures, with position of water table shown in blue for each panel. Red lines demonstrate thaw transition zone for the young bog and mature bog. (a) Stacked bar plot of methanogenic Archaea for all peat samples. Samples demonstrate significant differences in putative methanogen composition between all stages (Kruskall-Wallis test & Wilcox rank sum test, with Benjamini-Hochberg corrected p-values, $P < 0.05$). (b) Stacked bar plot of methanogenic Archaea for all pore water samples. Samples do not demonstrate significant differences in putative methanogen composition between stages (Kruskall-Wallis test, with Benjamini-Hochberg corrected p-values, $P = 0.965$).

Using a redundancy analysis (RDA, Figure 6) we found that 27.6% of variation in the methanogenic community was explained by two variables: thaw stage (ANOVA, $P < 0.05$) and depth from the water table (ANOVA, $P < 0.05$). Although these were the only two parameters that were identified as significant variables impacting microbial community structure when using a backward stepping model, it should be noted that there may be more variation in the community that our experimental design does not take into account as a result of unconstrained variation represented by plant-microbe and/or microbe-microbe interactions (Boon et al., 2014). Nonetheless, the 27.6% variation explained is in accordance with other studies conducted in permafrost impacted regions using similar methods, where the percentage of explained variation falls between 6% (low) to 43% (high) (Comte et al., 2015; Hough et al., 2020). Next, we used variance partitioning to assess the extent to which thaw stage and depth from the water table (i.e., the significant environmental variables identified by the RDA) explained the variation in only the methanogenic community structure (Figure 6). Based on this analysis, thaw stage explained 18.4% and distance to the water table explained 4.3% of methanogenic community variation, respectively.

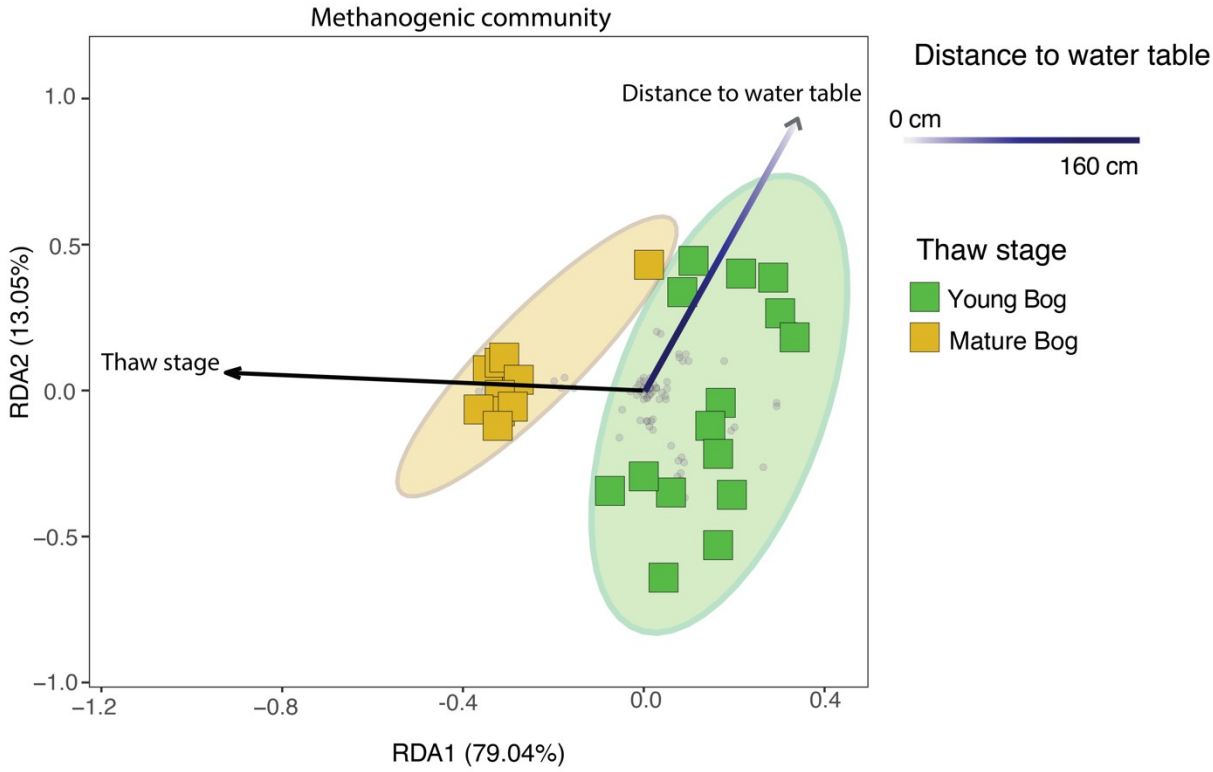


**Figure 6.** Redundancy analysis (RDA) exploring significant biotic and abiotic variables influencing the total methanogenic community (adjusted $R^2 = 27.6\%$), as determined by a backward stepping RDA model in the peat and pore water samples**.** All parameters that were used in model are described in section 2.10 of the Methods. Grey dots in the panel demonstrate the distribution of all ASVs in the methanogenic dataset. Shaded ellipses represent the 95% confidence intervals for microbial community structure according to peatland thaw stage (young bog vs mature bog). Only significant (ANOVA, $P < 0.05$) variables are shown. Using variation partitioning, we found that peatland thaw stage significantly explains about 18.4% of methanogenic community variation whereas distance to water table explained 4.3%. Both axes are significant (ANOVA, $P < 0.05$).

## 4. Discussion

Our study shows that high $CH_4$ emissions from thermokarst bogs in the initial decades following permafrost thaw (young bog) are not only linked to environmental conditions (wetness, soil temperature, vegetation), but also driven by relatively increased microbial $CH_4$

780 production through the energetically more favourable acetoclastic methanogenesis pathway.
781 Evidence of acetoclastic methanogens and $CH_4$ produced via the acetoclastic metabolic
782 pathway was found in the young bog both near the surface and at depths below the thaw
783 transition (i.e., in peat that accumulated prior to permafrost thaw). We are unable to
784 determine whether these greater $CH_4$ emissions in the initial decades following thaw are due
785 to the mineralization of labile organic matter released from previously frozen peat, or are
786 driven solely by fresh, labile DOM derived from surface vegetation leached throughout the
787 peat profile. However, previous work in the discontinuous permafrost region in the Interior
788 Plains of western Canada has found a limited contribution of previously frozen organic
789 matter contributing to surface $CH_4$ emissions in thermokarst bogs (Cooper et al., 2017).
790 Elevated $CH_4$ emissions then slow over the following centuries with succession into a mature
791 thermokarst bog stage where $CH_4$ production is almost exclusively through the
792 hydrogenotrophic pathway.

793 *4.1 Shift in microbial community assemblages along a permafrost thaw gradient*

794 Microbial communities varied along the permafrost thaw gradient; among different thaw
795 stages (permafrost peat plateau, young bog, and mature bog), with peat depth (surface down
796 to 160 cm), and between different sample types (solid peat and pore water). We found clear
797 differences in microbial communities between the young bog and mature bog, despite similar
798 peat stratigraphy up to the surficial vegetation (Heffernan et al., 2020), where dominant
799 *Sphagnum* species varied. The greater height of the peat surface above the water table and
800 drier conditions in the mature bog, due to the slow accumulation of new peat over centuries,
801 leads to a shift in vegetation composition from hydrophilic *Sphagnum* and graminoids
802 towards more drought resistant *Sphagnum* spp. and ericaceous shrubs. This shift in water
803 table position and vegetation community, along with a decrease in temperatures (Figure S1a)

804 due to the thermal insulating properties of *Sphagnum* peat (Kujala, Seppälä, & Holappa,
805 2008) appears to have caused the observed differences in microbial communities between the
806 young and mature bog, even at depths >1 m. Microbial communities were most dissimilar
807 between the peat plateau and young bog. This was unsurprising given the abrupt shift from
808 the elevated, frozen, and relatively dry peat plateau forest to the young bog where the surface
809 was saturated, dominated by hydrophilic vegetation and had warmer temperatures. We
810 further noted that the microbial community of the mature bog was more similar with the peat
811 plateau than with the young bog. Paleo-records in the region (Heffernan et al., 2020; Pelletier
812 et al., 2017; Zoltai, 1993) show that many peatlands have undergone cyclical permafrost
813 developments, as thermal insulating properties of *Sphagnum* peat in mature bogs leads to the
814 re-aggradation of permafrost peat plateaus. Our study suggests that the peat plateau microbial
815 community is influenced by the preceding mature bog microbial community as permafrost
816 aggrades.

817 The most dissimilar microbial community composition was observed between
818 samples near the surface and those at depth (i.e., down to 160 cm), as has also been
819 observed in other permafrost ecosystems (Frey et al., 2016; Monteux et al., 2018). Shifts in
820 microbial community composition along the thaw gradient were most evident nearer the
821 surface, whereas communities found at depth were similar between the young bog and mature
822 bog (Figure 4). At the surface, microbial community structure is influenced by the
823 successional vegetation community (Hodgkins et al., 2014) and the role that vegetation,
824 particularly graminoids which are found in the young bog, has on microbial community
825 structure has been well documented in northern peatlands (Robroek et al., 2015, 2021;
826 Bragazza et al., 2015). Moderately acidic, saturated peatlands with hydrophilic vegetation,
827 similar to the young bog, have been shown to harbour acid tolerant fermenting bacteria that
828 produce substrates for methanogenesis and are trophically linked with methanogens (Wüst et

al., 2009). Thus, the interaction between water table position, pH, and vegetation community influences the substrates available to the microbial community, which in turn impacts the surface community's structure (Kotiaho et al., 2013). In contrast, communities at depth are known to be influenced by peat properties, such as peat chemistry and degree of decomposition, and the paleoenvironment under which they originally colonized (Lee et al., 2012; Holm et al., 2020). In the young and mature bog both peat properties (humification indices including FTIR 1630/1090 $cm^{-3}$ and C:N ratios) and the paleoenvironment at depth are similar (Heffernan et al., 2020), which may explain the observed convergence of microbial community structure. Nonetheless, although there are some similarities at depth between both young and mature bog, microbial communities inhabiting either are still distinct (Figure 4). This is emphasized by the differing abundance of Archaea that participate in hydrogenotrophic or acetoclastic methanogenesis (Figure 5) in both stages down the peat profile.

As has been shown previously in other thermokarst peatlands (McCalley et al., 2014), the young and mature bog stages were dominated by hydrogenotrophic methanogens. However, acetoclastic methanogens were relatively more abundant in the young bog (Figure 5), particularly at or below the transition in peat that accumulated prior to permafrost thaw. Thaw stage and distance from the water table were found to influence the methanogenic community composition (Figure 6), with distance from the water table dictating where anoxic conditions persist (Blodau et al., 2004) and thus where methanogenic colonization can occur. The influence of vegetation communities associated with different thermokarst peatland stages on methanogenic community composition has previously been attributed to the role of plant derived DOM serving as the substrate for $CH_4$ production (Liebner et al., 2015; McCalley et al., 2014). The presence of hydrophilic vegetation, particularly graminoids, in the saturated young bog provides the precursors for fermentation, yielding acetate (Liebner et

854 al., 2015; Ström et al., 2003, 2012, 2015) and serving as the substrate for acetoclastic $CH_4$
855 production. The downward transport from the surface of plant derived DOM in the young
856 bog (Chanton et al., 2008) likely provides sufficient acetate for the establishment of
857 acetoclastic methanogens at depth in this environment.

858 *4.2 . Production and emissions of $CH_4$ along a peatland thaw gradient*

859 Isotopic signatures ($\delta^{13}C$) of dissolved $CO_2$ and $CH_4$ and $\alpha_C$ values in porewater and
860 the of $\delta^{13}C$ signature of $CH_4$ emitted to the atmosphere provided further evidence of
861 relatively elevated acetoclastic methanogenesis in the young bog stage. The general increase
862 in $\delta^{13}C$-$CO_2$ with depth observed at both sites (Figure 2d) indicates accumulation of
863 isotopically heavier $\delta^{13}C$-$CO_2$ which is likely explained by the preferential use of isotopically
864 lighter $\delta^{13}C$-$CO_2$ during hydrogenotrophic methanogenesis (Hornibrook et al., 2000). As a
865 result, $CH_4$ tends to become lighter with depth and this was particularly apparent in the
866 mature bog (Figure 2c). This leads to the average $\alpha_C$ values of 1.064 ($\delta^{13}C$-$CH_4$; -68.7‰) in
867 the mature bog, which were significantly higher than the 1.058 ($\delta^{13}C$-$CH_4$; -62.4‰) observed
868 in the young. Together, the $\delta^{13}C$-$CH_4$ and $\delta^{13}C$-$CO_2$ data and the resulting $\alpha_C$ depth profiles
869 suggest that the majority of $CH_4$ is produced via the hydrogenotrophic methanogenic
870 pathway, which supports the findings of the microbial community analysis (Figure 5). Our
871 isotope data also suggests that a greater proportion of $CH_4$ is produced via acetoclastic
872 methanogenesis throughout the profile in the young bog compared to the mature bog (Figure
873 2c – f). This is evident from lower average $\alpha_C$ values found in the young bog compared to the
874 mature bog, and greater number of these young bog $\alpha_C$ values falling between 1.040 – 1.065
875 which represents acetoclastic methanogenesis (Whiticar, 1999). These findings again agree
876 with the relatively greater abundance of acetoclastic methanogens observed at that site
877 (Figure 5).

878 In this study we found that average $CH_4$ emissions in the initial decades following thaw,
879 in the young bog stage, were 2.5 – 3 times greater than emissions measured in the mature bog
880 stage which had thawed ~200 years ago (Figure 3a). Furthermore, the proportion of $CH_4$ to
881 overall C emissions (Figure 3b) was considerably greater in the young bog than in the mature
882 bog. In the mature bog the lower water table position leads to both increased $CO_2$ emissions
883 and decreased $CH_4$ emissions, resulting in a reduced fraction of C emissions as $CH_4$. Previous
884 studies have shown similarly increased $CH_4$ emissions in the initial decades following thaw
885 (Johnston et al., 2014; Wickland et al., 2006). While our pore water chemistry data is
886 inconclusive with regards to organic carbon characteristics, other work in thermokarst bogs in
887 the Interior Plains of western Canada has shown that the organic matter derived from the
888 young bog vegetation community is highly labile (Burd et al., 2020). Previous work at our
889 study site has shown that the vegetation community in the young bog is associated with
890 greater potential enzymatic degradation of organic matter (Heffernan et al., 2021). Hydrolysis
891 of plant derived organic matter by extracellular enzymes leads to the formation of monomers
892 (Kotsyurbenko, 2005). These monomers can be further degraded to form acetate and other
893 percussors for methanogenesis when present with anaerobic fermenting bacteria (Hamberger
894 et al., 2008) and near the surface and vegetation inputs (Hädrich et al., 2012). Our study
895 shows that these higher $CH_4$ emissions are likely linked to increased wetness, temperatures,
896 and a vegetation community associated with more labile organic matter which favour a
897 greater proportion of $CH_4$ produced via acetoclastic methanogenesis, as shown by our $\delta^{13}C$-
898 $CH_4$, $\alpha_c$ depth profiles and microbial community composition analyses.
899 Many factors, including environmental conditions and microbial community structure
900 likely contribute to the differences in net $CH_4$ emissions from the young and mature bog
901 (Figure 3a). Methane oxidation has been shown to be an important regulator of post-thaw
902 $CH_4$ emissions (Perryman et al., 2020) and to result in isotopically heavier (i.e., less negative)

903 $\delta^{13}C\text{-}CH_4$ and lighter (i.e., more negative) $\delta^{13}C\text{-}CO_2$ (Whiticar, 1999). Our data suggests the
904 role of $CH_4$ oxidation was different between sites. Methane oxidation was apparent in the
905 $\delta^{13}C\text{-}CH_4$ and $\delta^{13}C\text{-}CO_2$ signatures above the water table in the mature bog but no $CH_4$
906 oxidation is evident in the young bog (Figure 2c, d). The difference in gas flux $\delta^{13}C$
907 signatures (Figure 3c) also suggests a greater prevalence of $CH_4$ oxidation in the mature bog.
908 However, increased oxidation above the water table in the mature bog is likely not fully
909 responsible for the observed differences in $CH_4$ surface emissions and depth profiles between
910 the young and mature bog. Lower soil temperatures, a vegetation community associated with
911 reduced substrate availability, the dominance of hydrogenotrophic methanogenesis
912 throughout the peat profile, and a deeper water table position all contribute to the lower $CH_4$
913 production and higher $CH_4$ oxidation observed in the mature bog. Nonetheless, using this
914 interdisciplinary approach, we are unable to determine the relative contribution of
915 acetoclastic methanogenesis at each depth to the overall emissions at the surface.
916 Our results, and those of others (Euskirchen et al., 2014; Johnston et al., 2014), have
917 shown that $CH_4$ emissions exhibit seasonal variation (Figure S3a, c) . However, in contrast to
918 some previous findings (Ebrahimi & Or, 2017), we did not observe a corresponding seasonal
919 response in the microbial community composition (Figure S2). This may be a sampling
920 design effect since our study spanned only two months (June and September), compounded
921 by the fact that we did not have replicate samples to test the robustness of this finding.
922 However, other studies have also shown that soil microbial community growth is not
923 impacted by seasonal variations in temperature (Simon et al., 2020) and that microbial
924 communities require a longer time scale (years-decades-centuries) to respond to temperature
925 following thaw (Feng et al., 2020). Our results corroborate these observations, suggesting a
926 long-term response in the microbial community composition to the ecological shifts
927 associated with autogenic peatland succession following permafrost thaw. Autogenic

928 peatland succession following thaw occurs on the decade to century timescale, shifting from
929 recently thawed to mature thermokarst bogs (Camill, 1999). Both recently thawed (young)
930 and mature thermokarst bogs have distinct hydrological regimes, vegetation communities,
931 and peat chemistry. Following thaw, associated changes in vegetation and litter input alters
932 microbial community composition and activity (Adamczyk et al., 2020; Kirkwood et al.,
933 2021). Such changes in microbial community structure thus impact $CH_4$ emissions from
934 thermokarst peatlands. Under predicted climatic warming scenarios differences in microbial
935 community composition have been shown to be increasingly driven by seasonally
936 independent variables such as substrate quality and the legacy effects of soil temperatures
937 (Luláková et al., 2019). This study suggests that the environmental conditions required for
938 increased methanogenic activity at depth is limited to the initial decades following thaw, after
939 which the microbial community structure changes in response to lowering of the water table,
940 lower soil temperatures and shifts in the vegetation community.

941 ## 5. Conclusion

942 This study demonstrates that higher $CH_4$ emissions in thermokarst bogs in the initial
943 decades following thaw are driven by shifts in vegetation communities that produce organic
944 matter inputs of varying lability (Burd et al., 2020) and prevalence of anoxic conditions,
945 which was associated with an increase of acetoclastic methanogenesis in our site. The
946 influence of this pathway was apparent at depth throughout the peat profile. With succession
947 following thaw towards a mature thermokarst bog, a shift in water table position and
948 vegetation composition seems to reduce the role of acetoclastic methanogenesis pathway.
949 Previous work at this site (Heffernan et al., 2021) and other thermokarst peatlands in the
950 discontinuous permafrost zone of boreal western Canada (Burd et al., 2020) have indicated
951 that the vegetation community found in the initial decades following permafrost thaw is

952 associated with increased potential enzymatic degradation and biodegradability of organic
953 matter compared to that found in the mature bog. Average growing season $CH_4$ emissions
954 were 2.5 – 3 times greater in the recently thawed young bog. Overall, C emissions in the
955 young bog contained proportionally more $CH_4$ than those from the mature bog, due to greater
956 $CH_4$ production and also reduced $CO_2$ emissions. These greater $CH_4$ emissions in the young
957 bog are driven by a higher contribution to surface emissions from $CH_4$ produced throughout
958 the peat profile by acetoclastic methanogens. The response of the microbial community to
959 permafrost thaw is tied to the shifting environmental conditions associated with peatland
960 autogenic succession. Warmer and wetter conditions in the initial decades following thaw, in
961 conjunction with a vegetation community associated with greater availability of labile plant
962 leachates (Bragazza et al., 2015), provides favourable conditions for acetoclastic
963 methanogens throughout the peat profile. Given the projected increases in thermokarst
964 peatland formation (Olefeldt et al., 2016), our study suggests that we can expect a pulse of
965 $CH_4$ emissions from current regions of the discontinuous permafrost zone. This pulse will be
966 driven, in part, by increased acetoclastic methanogenesis from labile substrates in recently
967 thawed thermokarst peatlands. However, this rapid increase in $CH_4$ emissions will only
968 remain at the decadal to century scale as autogenic peatland succession results in relatively
969 drier mature thermokarst bogs, where lower temperatures and less labile substrate availability
970 leads to a dominance of hydrogenotrophic methanogenesis.
971

972 **Data availability**

973 All biogeochemical and enzyme datasets generated and analyzed during this study are
974 available in the UAL Dataverse repository, [https://doi.org/10.5683/SP3/5TSH9V]. Microbial
975 sequences used in this study can be accessed from the NCBI database, using accession
976 number PRJNA660023.

977

978 **Author contributions**

979 All authors contributed to the conception of the work. LH and CEA performed the field work
980 component. LH performed the biogeochemistry measurements. MAC performed the
981 microbial measurements. LH and MAC analyzed the data and wrote the manuscript draft. All
982 authors reviewed and edited the manuscript.

983 **Competing interests**

984 The authors declare that they have no conflict of interest.

985 **Acknowledgements**

986 The authors wish to thank McKenzie Kuhn, Maya Frederickson, Jördis Stührenberg, and
987 Trisha Elliot for assistance with field and lab work. We also thank Sophie Dang, at MBSU
988 for providing guidance throughout 16S rRNA gene library building and for subsequently
989 sequencing these libraries at the MBSU facility.

990 **Financial support**

991 Funding and support were provided to D. Olefeldt and M. Bhatia by the Natural Science and
992 Engineering Research Council of Canada, Discovery grant (RGPIN-2016-04688 to DO and
993 RGPIN-2020-05975 to MB) and the Campus Alberta Innovates Program (CAIP).

994

995

996

997 ## References

Adamczyk, M., Perez-Mon, C., Gunz, S., & Frey, B. (2020). Strong shifts in microbial community structure are associated with increased litter input rather than temperature in High Arctic soils. Soil Biology and Biochemistry, 151. https://doi.org/10.1016/j.soilbio.2020.108054

Allan, E., Manning, P., Alt, F., Binkenstein, J., Blaser, S., Blüthgen, N., … Fischer, M. (2015). Land use intensification alters ecosystem multifunctionality via loss of biodiversity and changes to functional composition. Ecology Letters. https://doi.org/10.1111/ele.12469

Baltzer JL, Veness T, Chasmer LE, et al (2014) Forests on thawing permafrost: fragmentation, edge effects, and net forest loss. Global Change Biology 20:824–834. doi: 10.1111/gcb.12349

Bauer, I. E., Gignac, L. D., & Vitt, D. H. (2003). Development of a peatland complex in boreal western Canada: Lateral site expansion and local variability in vegetation succession and long-term peat accumulation. Canadian Journal of Botany, 81(8), 833–847. https://doi.org/10.1139/b03-076

Beilman, D. W. (2001). Plant community and diversity change due to localized permafrost dynamics in bogs of western Canada. Canadian Journal of Botany, 79(8), 983–993. https://doi.org/10.1139/cjb-79-8-983

Bellisario, L. M., Bubier, J. L., Moore, T. R., & Chanton, J. P. (1999). Controls on CH4 emissions from a northern peatland. Global Biogeochemical Cycles, 13(1). https://doi.org/10.1029/1998GB900021

Berghuis, B.A., Yu, F.B., Schulz, F., Blainey, P.C.,, Woyke, T., Quake, S.R. (2019). Hydrogenotrophic methanogenesis in archaeal phylum Verstraetearchaeota reveals the shared ancestry of all methanogens. PNAS 116 (11): 5037-5044. https://doi.org/10.1073/pnas.1815631116

Blodau, C., Basiliko, N., & Moore, T. R. (2004). Carbon turnover in peatland mesocosms exposed to different water table levels. Biogeochemistry. https://doi.org/10.1023/B:BIOG.0000015788.30164.e 2

Boon, E., Meehan, C. J., Whidden, C., Wong, D. H., Langille, M. G., & Beiko, R. G. (2014). Interactions in the microbiome: communities of organisms and communities of genes. FEMS microbiology reviews, 38(1), 90–118. https://doi.org/10.1111/1574-6976.12035

Bragazza, L., Bardgett, R. D., Mitchell, E. A. D., & Buttler, A. (2015). Linking soil microbial communities to vascular plant abundance along a climate gradient. New Phytologist, 205(3), 1175–1182. https://doi.org/10.1111/nph.13116

Bridgham, S. D., Cadillo-Quiroz, H., Keller, J. K., & Zhuang, Q. (2013). Methane emissions from wetlands: Biogeochemical, microbial, and modeling perspectives from local to global scales. Global Change Biology. https://doi.org/10.1111/gcb.12131

Brown, J., Ferrians Jr., O. J., Heginbottom, J. A., & Melnikov, E. S. (1997). Circum-Arctic map of permafrost and ground ice conditions. USGS Numbered Series, 1. https://doi.org/10.1016/j.jallcom.2010.03.054

Burd, K., Estop-Aragonés, C., Tank, S. E., & Olefeldt, D. (2020). Lability of dissolved organic carbon from boreal peatlands: interactions between permafrost thaw, wildfire, and season. Canadian Journal of Soil Science, 13(February), 1–13. https://doi.org/10.1139/cjss-2019-0154

Burger, M., Berger, S., Spangenberg, I., Blodau, C. (2016). Summer fluxes of methane and carbon dioxide from a pond and floating mat in a continental Canadian peatland. Biogeosciences. 13: 3777-3791. https://doi.org/10.5194/bg-13-3777-2016.

Cai, L., Alexeev, V.A., Arp, C.D., Jones, B.M., Liljedahl, A., Gadeke, A. (2016). Dynamical Downscaling data for studying climactic impacts on hydrology, permafrost and ecosystem sin Arctic Alaska. Earth System Science Data Discussion, doi:10.5194/tc-2016-87

Camill, P. (1999). Peat accumulation and succession following permafrost thaw in the Boreal peatlands of Manitoba, Canada. Ecoscience, 6(4), 592–602. https://doi.org/10.1080/11956860.1999.11682561

Carrigg, C., Rice, O., Kavanagh, S., Collins, G., O'Flaherty, V. (2007). DNA extraction method affects microbial community profiles from soils and sediment. Applied Microbiology and Biotechnology 77(4), 955-964.
Carroll, P., & Crill, P. (1997). Carbon balance of a temperate poor fen. Global Biogeochemical Cycles. https://doi.org/10.1029/97GB01365

Carson, M.A, Bräuer, S., Basiliko, N.,(2019). Enrichment of peat yields novel methanogens: approaches for obtaining uncultured organisms in the age of rapid sequencing, FEMS Microbiology Ecology, 95(2): https://doi.org/10.1093/femsec/fiz001

Chanton, J., Chaser, L., Glasser, P., & Siegel, D. (2005). Carbon and Hydrogen Isotopic Effects in Microbial, Methane from Terrestrial Environments. Stable Isotopes and Biosphere - Atmosphere Interactions, 85–105. https://doi.org/10.1016/B978-012088447-6/50006-4

Chanton, J. P., Glaser, P. H., Chasar, L. S., Burdige, D. J., Hines, M. E., Siegel, D. I., … Cooper, W. T. (2008). Radiocarbon evidence for the importance of surface vegetation on fermentation and methanogenesis in contrasting types of boreal peatlands. Global Biogeochemical Cycles, 22(4), 1–11. https://doi.org/10.1029/2008GB003274

Climate-Data.org. (2019). Retrieved January 21, 2019, from 2019 website: https://en.climate-data.org/north-america/canada/alberta/meander-river-11380/

Chasar, L. S., Chanton, J. P., Glaser, P. H., Siegel, D. I., and Rivers, J. S. (2000), Radiocarbon and stable carbon isotopic evidence for transport and transformation of dissolved organic carbon, dissolved inorganic carbon, and CH4 in a northern Minnesota peatland, Global Biogeochem. Cycles, 14( 4), 1095– 1108, doi:10.1029/1999GB001221.

Chasmer, L. and Hopkinson, C. (2017), Threshold loss of discontinuous permafrost and landscape evolution. Glob Change Biol, 23: 2672-2686. https://doi.org/10.1111/gcb.13537

Cooper, M. D. A., Estop-Aragonés, C., Fisher, J. P., Thierry, A., Garnett, M. H., Charman, D. J., et al. (2017). Limited contribution of permafrost carbon to methane release from thawing peatlands. Nature Climate Change, 7(7), 507–511. https://doi.org/10.1038/nclimate3328

Comte, J., Monier, A., Crevecoeur, S., Lovejoy,C., Vincent, W.F.(2015). Microbial biogeography of permafrost thaw ponds across the changing northern landscape. Ecography 39, 609-618.

Connon, R.F., Quinton, W.L., Craig, J.R., Hayashi, M. (2014). Changing hydrologic connectivity due to permafrost thaw in the lower Liard River valley, NWT, Canada. Hydrological Processes 28(14): 4163-4178. https://doi.org/10.1002/hyp.10206

Conrad, R. (1999). Contribution of hydrogen to methane production and control of hydrogen concentrations in methanogenic soils and sediments. FEMS Microbiology Ecology. https://doi.org/10.1016/S0168-6496(98)00086-5

Corbett, J. E., Tfaily, M. M., Burdige, D. J., Cooper, W. T., Glaser, P. H., & Chanton, J. P. (2013). Partitioning pathways of CO2 production in peatlands with stable carbon isotopes. Biogeochemistry, 114(1–3). https://doi.org/10.1007/s10533-012-9813-1

Criquet, S., Farnet, A. M., Tagger, S., & Le Petit, J. (2000). Annual variations of phenoloxidase activities in an evergreen oak litter: Influence of certain biotic and abiotic factors. Soil Biology and Biochemistry. https://doi.org/10.1016/S0038-0717(00)00027-4

Dunn, C., Jones, T.G, Girard, A., Freeman, C. (2014). Methodologies for Extracellular enzyme assays from wetland soils. Wetlands 34: 9-17 . https://doi.org/10.1007/s13157-013-0475-0.

Ebrahimi, A., & Or, D. (2017). Mechanistic modeling of microbial interactions at pore to profile scale resolve methane emission dynamics from permafrost soil. Journal of Geophysical Research: Biogeosciences, 122(5). https://doi.org/10.1002/2016JG003674

Euskirchen, E. S., Edgar, C. W., Turetsky, M. R., Waldrop, M. P., & Harden, J. W. (2014). Differential response of carbon fluxes to climate in three peatland ecosystems that vary in the presence and stability of permafrost. Journal of Geophysical Research G: Biogeosciences. https://doi.org/10.1002/2014JG002683

Feng, J., Wang, C., Lei, J., Yang, Y., Yan, Q., Zhou, X….Zhou, J. (2020). Warming-induced permafrost thaw exarcerbates tundra soil carbon decomposition mediated by microbial community. Microbiome 8(3), https://doi.org/10.1186/s40168-019-0778-3

Fisher, R. E., France, J. L., Lowry, D., Lanoisellé, M., Brownlow, R., Pyle, J. A., … Nisbet, E. G. (2017). Measurement of the 13C isotopic signature of methane emissions from northern European wetlands. Global Biogeochemical Cycles, 31(3). https://doi.org/10.1002/2016GB005504

Fox, J., & Weisberg, S. (2011). An R Companion to Applied Regression, second ed. https://doi.org/10.1016/j.stomax.2010.07.001

Frey, B., Rime, T., Phillips, M., Stierli, B., Hajdas, I., Widmer, F., Hartmann, M. (2016). Micorbial diversity in European alpine permafrost nad active layers. FEMS microbiology Ecology. 92: doi.org/10.1093/femsec/fiw018

Fritze, H., Penttilä, T., Mäkiranta, P., Laiho, R., Tuomivirta, T., Forsman, J., … Peltoniemi, K. (2021). Exploring the mechanisms by which reindeer droppings induce fen peat methane production. Soil Biology and Biochemistry, 160. https://doi.org/10.1016/j.soilbio.2021.108318

Galand, P. E., Fritze, H., Conrad, R., & Yrjälä, K. (2005). Pathways for methanogenesis and diversity of methanogenic archaea in three boreal peatland ecosystems. Applied and environmental microbiology, 71(4), 2195–2198. https://doi.org/10.1128/AEM.71.4.2195-2198.2005

Gibson, C. M., Chasmer, L. E., Thompson, D. K., Quinton, W. L., Flannigan, M. D., & amp. Olefeldt, D. (2018). Wildfire as a major driver of recent permafrost thaw in boreal peatlands. Nature Communications, 9(1). https://doi.org/10.1038/s41467-018-05457-1

Grant, R. F. (2015). Ecosystem CO2 and CH4 exchange in a mixed tundra and a fen within a hydrologically diverse Arctic landscape: 2. Modeled impacts of climate change. Journal of Geophysical Research: Biogeosciences, 120(7). https://doi.org/10.1002/2014JG002889

Hädrich, Anke., Heuer, Verena B., Herrmann, Martina., Hinrichs, Kai-Uwe., Küsel, Kirsten., Origin and fate of acetate in an acidic fen, FEMS Microbiology Ecology, Volume 81, Issue 2, August 2012, Pages 339–354, https://doi.org/10.1111/j.1574-6941.2012.01352.x

1173 Hamberger A, Horn MA, Dumont MG, Murrell JC & Drake HL (2008) Anaerobic consumers
1174 of monosaccharides in a moderately acidic fen. Appl Environ Microbiol 74: 3112–3120.
1175
1176 Hansen, A. M., Kraus, T. E. C., Pellerin, B. A., Fleck, J. A., Downing, B. D., & Bergamaschi,
1177 B. A. (2016). Optical properties of dissolved organic matter (DOM): Effects of biological and
1178 photolytic degradation. Limnology and Oceanography. https://doi.org/10.1002/lno.10270
1179
1180 Heffernan, L., Estop-Aragonés, C., Knorr, K.-H., Talbot, J., & Olefeldt, D. (2020).
1181 Long-term impacts of permafrost thaw on carbon storage in peatlands: deep losses offset by
1182 surficial accumulation. Journal of Geophysical Research: Biogeosciences, 2011(2865),
1183 e2019JG005501. https://doi.org/10.1029/2019JG005501
1184
1185 Heffernan, L., Jassey, V.E.J., Frederickson, M., Mackenzie, M.D., Olefeldt, D. (2021).
1186 Constraints on potential enzyme activities in thermokarst bogs: Implications for the carbon
1187 balance of peatlands following thaw. Global Change Biology, 27(19): 4711-4726.
1188 https://doi.org/10.1111/gcb.15758
1189
1190 Heginbottom, J. A., Dubreuil, M. H., & Harker, P. T. (1995). Canada, Permafrost. National
1191 Atlas of Canada.
1192
1193 Helbig, M., Pappas, C., & Sonnentag, O. (2016). Permafrost thaw and wildfire: Equally
1194 important drivers of boreal tree cover changes in the Taiga Plains, Canada. Geophysical
1195 Research Letters. https://doi.org/10.1002/2015GL067193
1196
1197 Helms, J.R., Stubbins, A., Ritchie, J.D., Minor, E.C., Kieber, D.J., Mopper, K. (2008).
1198 Absorption spectral slopes and slope rations as indicators of molecular weight, source, and
1199 photobleaching of chromophoric dissolved organic matter. Limnology and Oceanography,
1200 53(3): 955-969. https://doi.org/10.4319/lo.2008.53.3.0955
1201
1202 Hodgkins, S. B., Tfaily, M. M., McCalley, C. K., Logan, T. A., Crill, P. M., Saleska, S. R., …
1203 Chanton, J. P. (2014). Changes in peat chemistry associated with permafrost thaw
1204 increase greenhouse gas production. Proceedings of the National Academy of Sciences,
1205 111(16), 5819–5824. https://doi.org/10.1073/pnas.1314641111
1206
1207 Hoffman, G.E., Schadt, E.E. (2016). variancePartition: interpreting drivers of variance in
1208 complex gene expression studies. BMC bioinformatics 17(483).
1209 https://doi.org.10.1186/s12859-016-1323-z.
1210
1211 Holm, S., Walz, J., Horn, F., Yang, S., Grigoriev, M. N., Wagner, D., … Liebner, S. (2020).
1212 Methanogenic response to long-term permafrost thaw is determined by paleoenvironment.
1213 FEMS Microbiology Ecology, 96(3). https://doi.org/10.1093/femsec/fiaa021
1214
1215 Hopple, A. M., Wilson, R. M., Kolton, M., Zalman, C. A., Chanton, J. P., Kostka, J., …
1216 Bridgham, S. D. (2020). Massive peatland carbon banks vulnerable to rising

temperatures. Nature Communications, 11(1). https://doi.org/10.1038/s41467-020-16311-8

Hornibrook, E. R. C., Longstaffe, F. J., & Fyfe, W. S. (1997). Spatial distribution of microbial methane production pathways in temperate zone wetland soils: Stable carbon and hydrogen isotope evidence. Geochimica et Cosmochimica Acta, 61(4), 745–753. https://doi.org/https://doi.org/10.1016/S0016-7037(96)00368-7

Hornibrook, E. R. C., Longstaffe, F. J., & Fyfe, W. S. (2000). Evolution of stable carbon isotope compositions for methane and carbon dioxide in freshwater wetlands and other anaerobic environments. Geochimica et Cosmochimica Acta, 64(6). https://doi.org/10.1016/S0016-7037(99)00321-X

Hough, M., McClure, A., Bolduc, B., Dorrepaal, E., Saleska, S., Klepac-Ceraj, V., Rich, V. (2020). Biotic and environmental drivers of plant microbiomes across a permafrost thaw gradient. Frontiers in Microbiology: https://doi.org/10.3389/fmicb.2020.00796

Huang, Y., Ciais, P., Luo, Y., Zhu, D., Wang, Y., Qiu, C., … Qu, L. (2021). Tradeoff of CO2 and CH4 emissions from global peatlands under water-table drawdown. Nature Climate Change, 11(7). https://doi.org/10.1038/s41558-021-01059-w

Hugelius, G., Strauss, J., Zubrzycki, S., Harden, J. W., Schuur, E. A. G., Ping, C. L., … Kuhry, P. (2014). Estimated stocks of circumpolar permafrost carbon with quantified uncertainty ranges and identified data gaps. Biogeosciences, 11(23), 6573–6593. https://doi.org/10.5194/bg-11-6573-2014

Hugelius, G., Loisel, J., Chadburn, S., Jackson, R. B., Jones, M., MacDonald, G., Marushchak, M., Olefeldt, D., Packalen, M., Siewert, M. B., Treat, C., Turetsky, M., Voigt, C., & Yu, Z. (2020). Large stocks of peatland carbon and nitrogen are vulnerable to permafrost thaw. Proceedings of the National Academy of Sciences of the United States of America, 117(34), 20438–20446. https://doi.org/10.1073/pnas.19163 87117

Jassey, V. E. J., Chiapusio, G., Gilbert, D., Toussaint, M. L., & Binet, P. (2012). Phenoloxidase and peroxidase activities in Sphagnum-dominated peatland in a warming climate. Soil Biology and Biochemistry, 46, 49–52. https://doi.org/10.1016/j.soilbio.2011.11.011

Johnston, C. E., Ewing, S. A., Harden, J. W., Varner, R. K., Wickland, K. P., Koch, J. C., … Jorgenson, M. T. (2014). Effect of permafrost thaw on CO2 and CH4 exchange in a western Alaska peatland chronosequence. ENVIRONMENTAL RESEARCH LETTERS, 9(8). https://doi.org/10.1088/1748-9326/9/8/085004

Jones, M. C., Harden, J., O'Donnell, J., Manies, K., Jorgenson, T., Treat, C., & Ewing, S. (2017). Rapid carbon loss and slow recovery following permafrost thaw in boreal

peatlands. Global Change Biology, 23(3), 1109–1127. https://doi.org/10.1111/gcb.13403

Juottonen, H., Kieman, M., Fritze, H., Hamberg, L., Laine, A. M., Merilä, P., … Tuittila, E. S. (2021). Integrating Decomposers, Methane-Cycling Microbes and Ecosystem Carbon Fluxes Along a Peatland Successional Gradient in a Land Uplift Region. Ecosystems. https://doi.org/10.1007/s10021-021-00713-w

Kammann, C., Grünhage, L., & Jäger, H. J. (2001). A new sampling technique to monitor concentrations of CH4, N2O and CO2 in air at well-defined depths in soils with varied water potential. European Journal of Soil Science, 52(2). https://doi.org/10.1046/j.1365-2389.2001.00380.x

Kassambara, A., & Mundt, F. (2017). Package "factoextra." R Topics Documented.

Kassambara, A. (2018). ggpubr: "ggplot2" Based Publication Ready Plots. R package version 0.2. https://CRAN.R-project.org/package=ggpubr. Https://CRAN.R-Project.Org/Package=ggpubr. https://doi.org/R package version 0.1.8

Keeling, C. D. (1958). The concentration and isotopic abundances of atmospheric carbon dioxide in rural areas. Geochimica et Cosmochimica Acta, 13(4). https://doi.org/10.1016/0016-7037(58)90033-4

Kendall M.M., Boone D.R. (2006). Cultivation of methanogens from shallow marine sediments at Hydrate Ridge, Oregon. Archaea.2(1): 31-8. doi: 10.1155/2006/710190. PMID: 16877319; PMCID: PMC2685590.

Keuper, F., van Bodegom, P.M., Dorrepaal, E., Weedon, J.T., van Hal, J., van Logtestijn, R. S.P., Aerts, R. (2012). A frozen feast: thawing permafrost increases plant-available nitrogen in subarctic peatlands. Global Change Biology, 18(6) :1998-2007. https://doi.org/10.1111/j.1365-2486.2012.02663.x

Keuper, F., Dorrepaal, E., van Bodegom, P.M., van Logtesijn, R., Venhuizen, G., van Hal, J., Aerts, R. (2017). Experimentally increased nutrient availability at the permafrost thaw front selectively enhances biomass production of deep-rooting subarctic peatland species. Global Change Biology 23(10) : 4257-4266. doi: 10.1111/gcb.13804

Kirkwood, J. A. H., Roy-Léveillée, P., Mykytczuk, N., Packalen, M., McLaughlin, J., Laframboise, A., & Basiliko, N. (2021). Soil Microbial Community Response to Permafrost Degradation in Palsa Fields of the Hudson Bay Lowlands: Implications for Greenhouse Gas Production in a Warming Climate. Global Biogeochemical Cycles, 35(6). https://doi.org/10.1029/2021GB006954

Knoblauch, C., Beer, C., Liebner, S., Grigoriev, M.N., Pfeiffer, E.M. (2018). Methane production as key to the greenhouse gas budget of thawing permafrost. Nature Climate Change, 8, 309-312. https://doi.org/10.1038/s41558-018-0095-z

Knorr, K. H., Lischeid, G., & Blodau, C. (2009). Dynamics of redox processes in a minerotrophic fen exposed to a water table manipulation. Geoderma, 153(3–4). https://doi.org/10.1016/j.geoderma.2009.08.023

Kotiaho, M., Fritze, H., Merilä, P. et al. Actinobacteria community structure in the peat profile of boreal bogs follows a variation in the microtopographical gradient similar to vegetation. Plant Soil 369, 103–114 (2013). https://doi.org/10.1007/s11104-012-1546-3

Kotsyurbenko, O. R., Friedrich, M. W., Simankova, M. V., Nozhevnikova, A. N., Golyshin, P. N., Timmis, K. N., & Conrad, R. (2007). Shift from acetoclastic to H2-dependent methanogenesis in a West Siberian peat bog at low pH values and isolation of an acidophilic Methanobacterium strain. Applied and Environmental Microbiology, 73(7), 2344–2348. https://doi.org/10.1128/AEM.02413-06

Kotsyurbenko, O.R., (2005). Trophic interactions in the methanogenic microbial community of low-temperature terrestrial ecosystems, FEMS Microbiology Ecology. 53(1): 3–13, https://doi.org/10.1016/j.femsec.2004.12.009

Kuhn, M., Varner, R., Bastviken, D., Crill, P., MacIntyre, S., Turetsky, M., … Olefeldt, D. (2021). BAWLD-CH<sub>4</sub>: A Comprehensive Dataset of Methane Fluxes from Boreal and Arctic Ecosystems. Earth System Science Data Discussions. https://doi.org/10.5194/essd-2021-141

Kuhry, Peter (2008). Vegetation cover and radiocarbon dates of palsa and peat plateaus in the Hudson Bay Lowlands. PANGAEA, https://doi.org/10.1594/PANGAEA.812224, Supplement to: Kuhry, P (2008): Palsa and peat plateau development in the Hudson Bay Lowlands, Canada: timing, pathways and causes. Boreas, 37(2), 316-327, https://doi.org/10.1111/j.1502-3885.2007.00022.x

Kujala, K., Seppälä, M., & Holappa, T. (2008). Physical properties of peat and palsa formation. Cold Regions Science and Technology, 52(3). https://doi.org/10.1016/j.coldregions.2007.08.002

Lee, H., Schuur, E. A. G., Inglett, K. S., Lavoie, M., & Chanton, J. P. (2012). The rate of permafrost carbon release under aerobic and anaerobic conditions and its potential effects on climate. Global Change Biology, 18(2). https://doi.org/10.1111/j.1365-2486.2011.02519.x

Leroy, F., Gogo, S., Guimbaud, C., Bernard-Jannin, L., Hu, Z., & Laggoun-Défarge, F. (2017). Vegetation composition controls temperature sensitivity of CO2 and CH4 emissions

and DOC concentration in peatlands. Soil Biology and Biochemistry, 107. https://doi.org/10.1016/j.soilbio.2017.01.005

Liebner, S., Ganzert, L., Kiss, A., Yang, S., Wagner, D., &; Svenning, M. M. (2015). Shifts in methanogenic community composition and methane fluxes along the degradation of discontinuous permafrost. Frontiers in Microbiology, 6(MAY). https://doi.org/10.3389/fmicb.2015.00356

Lin, Y., Liu, D., Yuan, J., Ye, G,m Ding, W. (2017). Methanogenic community was stable in two contrasting freshwater marshes exposed to elevated atmospheric CO2. Front Microbiol. https://doi.org/10.3389/fmicb.2017.00932

Luláková, P., Perez-Mon, C., Šantrůčková, H., Ruethi, J., &; Frey, B. (2019). High-alpine permafrost and active-layer soil microbiomes differ in their response to elevated temperatures. Frontiers in Microbiology, 10(APR). https://doi.org/10.3389/fmicb.2019.00668

Masella, A. P., Bartram, A. K., Truszkowski, J. M., Brown, D. G., & Neufeld, J. D. (2012). PANDAseq : PAired-eND Assembler for Illumina sequences. (Figure 1), 1–7.

McCalley, C. K., Woodcroft, B. J., Hodgkins, S. B., Wehr, R. A., Kim, E. H., Mondav, R., … Saleska, S. R. (2014). Methane dynamics regulated by microbial community response to permafrost thaw. Nature, 514(7253), 478–481. https://doi.org/10.1038/nature13798

McDonald, D., Price, M.N., Goodrich, J., Nawrocki, E.P., DeSantis,, T.Z., Probst, A., Andersen, G.L., Knight, R., Hugenholtz, P. (2012). An improved Greengenes taxonomy with exzplicit ranks for ecological and evolutionary analyses of bacteria and archaea. ISME Journal 6: 610-618. https://doi.org/10.1038/ismej.2011.139

McNicol, G., Knox, S.H., Guilderson, T.P.., Baldocchi, D.D., Silver, W.L. (2019). Where old meets new: An ecosystem study of methanogenesis in a reflooded agricultural peatland. Global Change Biology 26(2):772-785.

Monteux, S., Weedon, J. T., Blume-Werry, G., Gavazov, K., Jassey, V. E. J., Johansson, M., … Dorrepaal, E. (2018). Long-term in situ permafrost thaw effects on bacterial communities and potential aerobic respiration. ISME Journal. https://doi.org/10.1038/s41396-018-0176-z

Mudryk, L., Brown, R., Derksen, C., Luojus, K., Decharme, B., & Helfrich, S. (2018). Surface Air Temperature [in Arctic Report Card 2018]. Retrieved from https://www.arctic.noaa.gov/Report-Card

Nielsen, C.S,. Hasselquist, N.J, Nilsson, M.B., Öquist M., Järveoja J., Peichl M .(2019) .A Novel Approach for High-Frequency in-situ Quantification of Methane Oxidation in Peatlands. Soil Systems 3: 4

Oksanen, J., Blanchet, F. G., Kindt, R., Oksanen, M. J., & Suggests, M. (2013). Package 'vegan.' Community Ecology Package Version.

Olefeldt, D., Goswami, S., Grosse, G., Hayes, D., Hugelius, G., Kuhry, P., … Turetsky, M. R. (2016). Circumpolar distribution and carbon storage of thermokarst landscapes. Nature Communications, 7, 13043. https://doi.org/10.1038/ncomms13043

Olefeldt, D., Euskirchen, E. S., Harden, J., Kane, E., McGuire, A. D., Waldrop, M. P., & Turetsky, M. R. (2017). A decade of boreal rich fen greenhouse gas fluxes in response to natural and experimental water table variability. Global Change Biology, 23(6), 2428–2440. https://doi.org/10.1111/gcb.13612

Olefeldt, D., Heffernan, L., Jones, M. C., Sannel, A. B. K., Treat, C. C., & Turetsky, M. R. (2021). Permafrost thaw in northern peatlands: rapid changes in ecosystem and landscape functions. Ecosystem Collapse and Climate Change, 27-67.

Parada, A. E., Needham, D. M., & Fuhrman, J. A. (2016). Every base matters: assessing small subunit rRNA primers for marine microbiomes with mock communities, time series and global field samples. 18, 1403–1414. https://doi.org/10.1111/1462-2920.13023

Pelletier, N., Talbot, J., Olefeldt, D., Turetsky, M., Blodau, C., Sonnentag, O., & Quinton, W. L. (2017). Influence of Holocene permafrost aggradation and thaw on the paleoecology and carbon storage of a peatland complex in northwestern Canada. Holocene, 27(9), 1391–1405. https://doi.org/10.1177/0959683617693899

Perryman, C. R., McCalley, C. K., Malhotra, A., Fahnestock, M. F., Kashi, N. N., Bryce, J. G., … Varner, R. K. (2020). Thaw Transitions and Redox Conditions Drive Methane Oxidation in a Permafrost Peatland. Journal of Geophysical Research: Biogeosciences, 125(3). https://doi.org/10.1029/2019JG005526

Pinheiro J, Bates D, DebRoy S, S. D. and R. C. T. (2017). nlme: Linear and Nonlinear Mixed Effects Models. R package version 3.1-131, https://CRAN.R-project.org/package=nlme. R Package Version 3.1-131, Https://CRAN.R-Project.Org/Package=nlme. https://doi.org/10.1016/j.tibs.2011.05.003

Popp, T. J., Chanton, J. P., Whiting, G. J., and Grant, N. (1999), Methane stable isotope distribution at a Carex dominated fen in north central Alberta, Global Biogeochem. Cycles, 13( 4), 1063– 1077, doi:10.1029/1999GB900060.

Preuss I, Knoblauch C, Gebert J & Pfeiffer EM (2013) Improved quantification of microbial CH4 oxidation efficiency in arctic wetland soils using carbon isotope fractionation. Biogeosciences 10: 2539-2552

Quince, C., Lanzen, A., Davenport, R. J., & Turnbaugh, P. J. (2011). Removing Noise From Pyrosequenced Amplicons.

R Core Team. (2015). R: A language and environment for statistical computing. Vienna, Austria; 2014. URL Http://Www. R-Project. Org. Vienna, Austria: R Foundation for Statistical Computing. https://doi.org/10.1007/978-3-540-74686-7

Robroek, B. J. M., Jassey, V. E. J., Kox, M. A. R., Berendsen, R. L., Mills, R. T. E., Cécillon, L., … Bodelier, P. L. E. (2015). Peatland vascular plant functional types affect methane dynamics by altering microbial community structure. Journal of Ecology, 103(4). https://doi.org/10.1111/1365-2745.12413

Robroek, B. J. M., Martí, M., Svensson, B. H., Dumont, M. G., Veraart, A. J., & Jassey, V. E. J. (2021). Rewiring of peatland plant–microbe networks outpaces species turnover. Oikos, 130(3). https://doi.org/10.1111/oik.07635

Schädel, C., Bader, MF., Schuur, E. et al. Potential carbon emissions dominated by carbon dioxide from thawed permafrost soils. Nature Clim Change 6, 950–953 (2016). https://doi.org/10.1038/nclimate3054

Schaefer, K., Zhang, T., Bruhwiler, L., & Barrett, A. P. (2011). Amount and timing of permafrost carbon release in response to climate warming. Tellus, Series B: Chemical and Physical Meteorology, 63(2). https://doi.org/10.1111/j.1600-0889.2011.00527.x

Schuur, E. A. G., McGuire, A. D., Schädel, C., Grosse, G., Harden, J. W., Hayes, D. J., … Vonk, J. E. (2015). Climate change and the permafrost carbon feedback. Nature, 520(7546), 171–179. https://doi.org/10.1038/nature14338

Simon, E., Canarini, A., Martin, V., Séneca, J., Böckle, T., Reinthaler, D., … Richter, A. (2020). Microbial growth and carbon use efficiency show seasonal responses in a multifactorial climate change experiment. Communications Biology, 3(1). https://doi.org/10.1038/s42003-020-01317-1

Strack, M., Waddington, J. M., & Tuittila, E. S. (2004). Effect of water table drawdown on northern peatland methane dynamics: Implications for climate change. Global Biogeochemical Cycles. https://doi.org/10.1029/2003GB002209

Stams A.J.M., Teusink B., Sousa D.Z. (2019) Ecophysiology of Acetoclastic Methanogens. In: Stams A., Sousa D. (eds) Biogenesis of Hydrocarbons. Handbook of Hydrocarbon and Lipid Microbiology. Springer, Cham. https://doi.org/10.1007/978-3-319-78108-2_21

Ström, L., Ekberg, A., Mastepanov, M. and Røjle Christensen, T. (2003), The effect of vascular plants on carbon turnover and methane emissions from a tundra wetland. Global Change Biology, 9: 1185-1192. https://doi.org/10.1046/j.1365-2486.2003.00655.x

Ström et al., (2012). Presence of Eriophorum scheuchzeri enhances substrate availability and methane emission in an Arctic wetland Soil Biology and Biochemistry 45: 61-70, ISSN 0038-0717, https://doi.org/10.1016/j.soilbio.2011.09.005.

Strom, L., Falk, J.M., Skov, K., Jackowizc-Korczynski, M., Mastepanov, M., Christensen, T., Lund, M., Schmidt, N.M. (2015). Controls of spatial and temporal variabilirt in CH4 flux in a high arctic fen over three years. Biogeochemistry 125(1): 21-35.

Turetsky, M. R., Wieder, R. K., Vitt, D. H., Evans, R. J., & Scott, K. D. (2007). The disappearance of relict permafrost in boreal north America: Effects on peatland carbon storage and fluxes. Global Change Biology, 13(9), 1922–1934. https://doi.org/10.1111/j.1365-2486.2007.01381.x

Turetsky, Merritt R., Abbott, B. W., Jones, M. C., Anthony, K. W., Olefeldt, D., Schuur, E. A. G., … McGuire, A. D. (2020). Carbon release through abrupt permafrost thaw. Nature Geoscience. https://doi.org/10.1038/s41561-019-0526-0

Tuittila, E. S., Komulainen, V. M., Vasander, H., Nykanen, H., Martikainen, P. J., & Laine, J. (2000). Methane dynamics of a restored cut-away peatland. Global Change Biology, 6(5), 569–581. https://doi.org/10.1046/j.1365-2486.2000.00341.x

Vanwonterghem, I., Evans, P., Parks, D. et al. (2016). Methylotrophic methanogenesis discovered in the archaeal phylum Verstraetearchaeota. Nat Microbiol 1: https://doi.org/10.1038/nmicrobiol.2016.170

Vishnivetskaya, T.A., Buongiorno, J., Bird, J., Krivushin, K., Spirina, E.V., Oshurkova, V., Shcherbakova, V.A., Wilson, G., Lloyd, K.G., Rivkina, E.M. (2018).Methanogens in the Antarctic Dry Valley permafrost, *FEMS Microbiology Ecology*, 94( 8) fiy109, https://doi.org/10.1093/femsec/fiy109

Vitt, D. H., Halsey, L. A., Bauer, I. E., & Campbell, C. (2000). Spatial and temporal trends in carbon storage of peatlands of continental western Canada through the Holocene. Canadian Journal of Earth Sciences, 37(5), 683–693. https://doi.org/10.1139/e99-097

Vitt, D. H., Halsey, L. A., & Zoltai, S. C. (1994). The Bog Landforms of Continental Western Canada in Relation to Climate and Permafrost Patterns. Arctic and Alpine Research, 26(1), 1. https://doi.org/10.2307/1551870

Weishaar, J.L., Aiken, G.R., Bergamaschi, B.A., Fram, M.S., Fujii, R., Mopper, K. (2003). Evaluation of specific ultraviolet absorbance as an indicator of the chemical composition and reactivity of dissolved organic carbon. Environmental Science and Technology 37(20): 4702-4708. https://doi.org/10.1021/es030360x

Whiticar, M. J., Faber, E., & Schoell, M. (1986). Biogenic methane formation in marine and freshwater environments: CO2 reduction vs. acetate fermentation-Isotope evidence. Geochimica et Cosmochimica Acta, 50(5). https://doi.org/10.1016/0016-7037(86)90346-7

Whiticar, Michael J. (1999). Carbon and hydrogen isotope systematics of bacterial formation and oxidation of methane. Chemical Geology, 161(1). https://doi.org/10.1016/S0009-2541(99)00092-3

Wickham, H. (2016). ggplot2 -Positioning Elegant Graphics for Data Analysis. In Springer.

Wickland, K. P., Striegl, R. G., Neff, J. C., & Sachs, T. (2006). Effects of permafrost melting on CO2 and CH4 exchange of a poorly drained black spruce lowland. Journal of Geophysical Research: Biogeosciences, 111(2), 1–13. https://doi.org/10.1029/2005JG000099

Wüst, P.K., Horn, M.A. and Drake, H.L. (2009), Trophic links between fermenters and methanogens in a moderately acidic fen soil. Environmental Microbiology, 11: 1395-1409. https://doi.org/10.1111/j.1462-2920.2009.01867.x

Ye, R., Jin, Q., Bohannan, B., Keller, J. K., McAllister, S. A., & Bridgham, S. D. (2012). PH controls over anaerobic carbon mineralization, the efficiency of methane production, and methanogenic pathways in peatlands across an ombrotrophic-minerotrophic gradient. Soil Biology and Biochemistry, 54, 36–47. https://doi.org/10.1016/j.soilbio.2012.05.015

Zhang, CJ., Pan, J., Liu, Y. et al. (2020). Genomic and transcriptomic insights into methanogenesis potential of novel methanogens from mangrove sediments. Microbiome 8 (94 ): https://doi.org/10.1186/s40168-020-00876-z

Zoltai, S. C. (1972). Palsas and Peat Plateaus in Central Manitoba and Saskatchewan. Canadian Journal of Forest Research, 2(3), 291–302. https://doi.org/10.1139/x72-046

Zoltai, S. C. (1993). Cyclic Development of Permafrost in the Peatlands of Northwestern Alberta, Canada. Arctic and Alpine Research, 25(3), 240. https://doi.org/10.2307/1551820